Exploring dystrophin-mediated control of neural stem cell fate associated with intellectual disability in Duchenne Muscular Dystrophy patients

Shannon Thompson

Thesis Submitted to the
Faculty of Graduate and Postdoctoral Studies
in partial fulfillment of requirements
for the M.Sc degree in Neuroscience

Department of Cellular and Molecular Medicine
Faculty of Medicine
University of Ottawa

ABSTRACT

Duchenne Muscular Dystrophy (DMD) is an X-linked recessive neuromuscular disease characterized by progressive muscle-wasting and loss of mobility. One-third of patients with DMD are also affected by cognitive impairments such as a lower than average IQ and impaired working memory, comorbid with neuropsychiatric disorders such as anxiety and autism-related behaviours. DMD is caused by mutations in the *DMD* gene resulting in the deletion of the full-length dystrophin protein (Dp427) and, dependent on mutation, other dystrophin isoforms. These isoforms are predominantly found in the brain and deletion may impact on cognition. The most commonly used animal model to study DMD is the *mdx* mouse which completely lacks Dp427 but no other DMD isoforms. Although the muscle phenotype is well-established, behavioural characterization of the *mdx* mouse model has been inconclusive. In this thesis I investigated the hippocampal and amygdala cellular and behavioural phenotypes of the *mdx* mouse. I show that post-natal neural stem-like cell division in the SGZ is altered in the absence of Dp427 resulting in enhanced symmetric division. I show *in vitro* that primary *mdx* cultures are fewer and smaller than wild-type, consistent with an increase in symmetrical self-renewal whereas secondary cultures are fewer and larger, consistent with a shift in symmetric division producing transit-amplifying type 2a daughter cells. I next characterized the *mdx* mouse model using a battery of behavioural tests. Data presented here show that *mdx* mice do not exhibit an anxious phenotype, do not display autism-related behaviours, and do not display impairments in and spatial learning or memory. However, associative learning, as measured in the fear conditioning paradigm is enhanced in *mdx* mice. Lastly, I attempted to generate three different brain-specific dystrophin knock-out mouse models to examine role of other dystrophin isoforms. While none of the models were able to deplete dystrophin from brain, given the inverse relationship between Cre-mediated efficiency and

the genetic distance of the loxP sites in the fDMDH mouse employed, I do provide important insight into the presence and absence of the muscle-specific enhancers in constructs commonly used to generate brain-specific mouse models. Taken together, this thesis provides converging evidence to indicate that loss of Dp427 impacts on fear associative learning and stem-cell like division in the SGZ but likely does not underlie the non-progressive cognitive impairments affecting one-third of all DMD patients.

ACKNOWLEDGEMENTS

To: Dr. Steffany Bennett,

Thank you for accepting me into your lab two years ago and challenging me day in day out to be a better scientist and (more articulate) person.

To: The Neural Regeneration Laboratory,

Thank you for everything over the last 2 years - the moral support, the endless encouragement and the guidance, through thick and thin. I have learned many invaluable lessons while in the NRL lab, and it's all because of this amazing team. You are all incredible people that I'm proud to call my friends.

To: The Jersey Boys Soundtrack,

Thanks for being my emotional crutch throughout the course of the thesis-writing/defending process.

TABLE OF CONTENTS

LIST OF ABBREVIATIONS

ACSF	Artificial Cerebrospinal Fluid
ADHD	Attention Deficit Hyperactive Disorder
ASD	Autism Spectrum Disorder
ANSC	Adult Neural Stem-like Cell
BSA	Bovine Serum Albumin
BLA	Basolateral Amygdala
CNS	Central Nervous System
CR	Cysteine-Rich Domain
CT	C-Terminal
CV	Chemical Variant
DAPC	Dystrophin Associated Protein Complex
DCX	Doublecortin
dB	Decibel
DG	Dentate Gyrus
DMD	Duchenne Muscular Dystrophy
DMD	Duchenne Muscular Dystrophy gene
DIV	Days In Vitro
Dp	Dystrophin Protein
ECM	Extracellular Matrix
EGF	Epidermal Growth Factor
EPM	Elevated Plus Maze
FC	Fear Conditioning
FGF	Fibroblast Growth Factor
FIQ	Full-Scale Intelligence Quotient
GABA	Gamma-aminobutyric acid
GFAP	Glial Fibrillary Acidic Protein
IFC	Immunofluorescence and confocal microscopy
i.p	Intraperitoneal
kDa	Kilodalton
Mark2	MAP/microtubule affinity-regulating kinase 2
MB	Marble Burying
MWM	Morris Water Maze
LDB	Light Dark Box
NB	Nest Building
NLGN1	Neurolgin-1
NLGN2	Neuroligin-2
NPC	Neural Progenitor Cell
NSP	Neurosphere
NT	N-Terminal
OCD	Obsessive Compulsive Disorder
OF	Open Field
PBS	Phosphate Buffered Saline
PFA	Paraformaldehyde

PVC	Polyvinylchloride
SGZ	Subgranular Zone
SVZ	Subventricular Zone
TA	Tibialis Anterior
TAM	Tamoxifen
WT	Wild-Type
ZT	Zeitgeber

LIST OF FIGURES

LIST OF TABLES

1 INTRODUCTION

1.1 Duchenne Muscular Dystrophy (DMD) is an X-linked debilitating neuromuscular disease caused by mutations in the *DMD* gene

Duchenne Muscular Dystrophy (DMD) is an X-linked recessive neuromuscular disease characterized by progressive muscle-wasting and loss of mobility, affecting 1:3500 newborn males (Blake, 2002). Affected children have delayed milestones in motor skill development, as well as difficulty walking, imbalance, and Gower's sign (weakness in proximal muscles; (Mehler, 2000; Blake, 2002). Progressive muscle fibre necrosis causes children to become wheel-chair dependent typically by 12 years of age, and predisposes them to cardiomyopathy and respiratory failure, shortening their life expectancy to the third decade of life (Blake, 2002; Chang et al., 2016). The quality of life of DMD patients is drastically reduced by disease severity and related symptoms (pain, fatigue and mood; (Pangalila et al., 2015), emphasizing the importance of therapeutic relief for those affected by DMD.

The 2.5 Mb *DMD* gene, the largest gene in the human genome, is the genetic determinant of DMD (Blake, 2002). This gene is comprised of 79 exons (Chang et al., 2016). Mutations causing the loss of the full-length 427 kDa cytoplasmic dystrophin protein (Dp427; ((Krasowska et al., 2014)) result in DMD. Dp427 is found predominantly in skeletal and cardiac muscle (Chang 2016), as well as in smooth muscle and the brain (Chang et al., 2016). Dystrophin protein is composed of four domains: 1) the N-terminal (NT), with many actin-binding sites, 2) the rod domain containing 24-spectrin helical coils that bridge the NT-domain with the 3) cysteine-rich (CR) domain, and 4)a C-terminal (CT), highly homologous across species (Mehler, 2000; Ehmsen et al., 2002; McGreevy et al., 2015). The CR-domain contains (a) two EF-hand motifs, binding intracellular calcium, and (b) a ZZ-domain, which binds calmodulin in a calcium-dependent

manner (Mehler, 2000; Blake, 2002). Deletions within the CR result are associated with severe DMD phenotypes (Mehler, 2000). In contrast, mutations in the rod domain appear to be relatively benign. Dp427 is functional with as few as 8 spectrin repeats (Ehmsen et al., 2002). The C-terminus of Dp427 possesses a WW-domain mediating the interaction between dystrophin with extracellular also referred to as peripheral (dystrobrevins and syntrophins) and transmembrane (sarcoglycan, dystroglycan and sarcospan) proteins which form the dystrophin associated protein complex (DAPC; (Blake, 2002; Waite et al., 2009; McGreevy et al., 2015)).

The composition and function of the DAPC differ in muscle and in brain (Waite et al., 2009). In muscle, DAPC links the actin cytoskeleton to the extracellular matrix (ECM) to stabilize the sarcolemma during repeated cycles of contraction and relaxation, consequently protecting the sarcolemma from damage (Ehmsen et al., 2002). In the absence of Dp427, DAPC does not form, resulting in disruption of the link between cytoskeletal proteins and ECM, causing muscle fibre damage, chronic inflammation, and progressive muscle weakness (Blake, 2002; Waite et al., 2009; Snow et al., 2013; Takos and Rook, 2013). As well, the DAPC has a role in regulating intracellular calcium homeostasis (Blake, 2002). In the absence of dystrophin, intracellular calcium concentrations are raised, activating calcium-dependent proteases, resulting in cellular damage that leads to apoptosis and necrosis (Blake, 2002; Hollinger and Selsby, 2013).

In the brain, DAPC has the central role in regulating and modulating the molecular machinery of synapses (Krasowska et al., 2014). Dystrophin is expressed over the course of brain development within the neural tube and is hypothesized to regulate multiple aspects of neurogenesis including neuronal migration and cellular differentiation (Mehler, 2000). In the adult brain, DAPC contributes to anchoring neurotransmitter receptors to post-synaptic densities

(Krasowska et al., 2014) and plays a role in synaptic plasticity and regional cell signal integration (Mehler, 2000).

Multiple DMD isoforms are generated by either alternate or tissue-specific promoters and/or splicing variants. To date, seven DMD promoters have been identified, each named for their primary tissue of expression (Blake, 2002; Doorenweerd et al., 2017). For example, Dp427(B) is the promoter driving expression of the full-length dystrophin protein in the brain (Mehler, 2000). Multiple promoters in addition to alternative splicing give rise to 17 unique isoforms. These are named according to the protein mass (Doorenweerd et al., 2017). Most, if not all, information regarding dystrophin isoforms have been from animal models. Table 1 highlights the expression pattern of each dystrophin isoform in adult humans; comparatively, table 2 shows where dystrophin is found in mouse models. Although the smaller isoforms are expressed in different cell types and regions throughout the body (Blake, 2002), they are mainly found in the brain and have implications in cognitive function (Krasowska et al., 2014). In healthy individuals, Dp427 and its smaller isoforms are expressed in regions of the brain involved in cognitive functioning, including the hippocampus, cerebral cortex, amygdala and cerebellum (Mehler, 2000; Wicksell et al., 2004; Miranda et al., 2016). In DMD patients, Dp427 is not detected in cerebrum nor cerebellum (Uchino et al., 1994) and patients exhibit a disordered architecture of the central nervous system (CNS; (Hendriksen and Vles, 2008)), including neurofibrillary tangles, abnormalities in dendritic length and branching, fewer neurons, and smaller brain volumes with a reduction in grey matter (Anderson et al., 2002; Hendriksen and Vles, 2008; Banihani et al., 2015).

Table 1 Human dystrophin isoforms, sizes, and locations of expression

Isoform	Molecular Weight (g/mol)	Location	Reference (s)
Dp427B (brain)	427, 000	Brain (cerebral, cortical, amygdalar mature neurons); CA hippocampal neurons but not in granule cells; stellate neurons; astrocytes; retina	Mehler, 2000(Nudel et al., 1989)
Dp427M (muscle)	427, 000	Skeletal muscle (sarcolemma); heart muscle (cardiomyocytes); CNS glial cells; vascular endothelial cells	Mehler, 2000
Dp427P (Purkinje cells)	427, 000	Purkinje Cells	Mehler, 2000
Dp260	260, 000	Retina (virtually exclusively – found on retinal photoreceptor cells and ON bipolar cells)	Mehler, 2000; Waite, 2009
Dp140	140, 000	Microvasculature; glial cells (astrocytes); cerebellum; kidney; retina	Lidov, 1995; Blake, 2002; Mehler, 2000; Waite 2009,
Dp116	116, 000	Schwann cells of Peripheral Nervous System (not associated with myelinated structures in adult CNS)	Mehler, 2000; Waite, 2009
Dp71	71, 000	Ubiquitous – except absent in skeletal muscle; brain (neuron and astrocytes); kidney; liver; testis and lung; Glial cells (perivascular astrocytes and Bergmann glia)	Blake, 2002; Mehler, 2000
Dp40	40, 000	Glial cells (perivascular astrocytes and Bergmann glia)	Waite, 2009

Table 2 Mouse dystrophin isoforms, sizes and locations of expression

Isoform	Molecular Weight (g/mol)	Location	Reference (s)
Dp427B (brain)	427, 000	Brain (cortical neurons and CA regions of hippocampus)	(Nudel et al., 1989; Lidov, 2000)
Dp427L	427, 000	Lymphoblastoid cells	(Muntoni et al., 1993; Nishio et al., 1994)
Dp427M (muscle)	427, 000	Skeletal muscle (sarcolemma); heart muscle (cardiomyocytes); CNS glial cells; vascular endothelial cells	Mehler, 2000
Dp427P1 (Purkinje cells)	427, 000	Purkinje Cells (cerebellum), skeletal muscle, heart	Holder, 1996
DP417P2 (Purkinje cells)	427, 000	Purkinje Cells (cerebellum), skeletal muscle, heart	
Dp260	260, 000	Retina	(D'Souza et al., 1995)
Dp140	140, 000	Fetal development	doorenweerd
Dp116	116, 000	PNS	Byers, 1993
Dp71	71, 000	Ubiquitous, highest in CNS, testes, lung, kidney, brain liver	Doorenweerd, 2017; Bar, 1990

1.1.1 The *mdx* mouse model is the most commonly used animal model to study DMD

Discovered in 1984 by Bulfield *et al*, the *mdx* mouse is the most commonly used animal model to study DMD (Miranda et al., 2016). In contrast to human patients, where intragenic deletions or duplications disrupt the translational reading frame and completely abolishes Dp427 (Mehler, 2000), the *mdx* mouse has a nonsense point mutation (C-to-T transition) at exon 23 that introduces a premature stop codon, resulting in the complete loss of Dp427 in murine muscle and brain (figure 1; McGreevy et al., 2015; Miranda et al., 2016). Although both DMD patients and *mdx* mice are devoid of Dp427, there are differences between their clinical and experimental phenotypes (McGreevy et al., 2015).

Hemizygous *mdx* males and homozygous females have a lifespan that is reduced by ~25%, compared to the ~75% reduced lifespan of DMD patients (McGreevy et al., 2015; Remmelink et al., 2016). The *mdx* mice also have less severe myopathy than DMD patients (Vaillend et al., 1995). Patients 3-5 years of age exhibit elevated levels of serum creatine kinase, a marker for muscle decay and necrosis of skeletal myofibers (Blake, 2002; Sun et al., 2008). During this period there is active muscle regeneration to replace and repair lost or damaged fibres (Blake, 2002). However, the regenerative capacity of muscle is eventually lost, attributed to limited proliferative capacity of satellite cells (Klingler et al., 2012). This results in muscle fibre being replaced with adipose and fibrous connective tissue and gives rise to pseudohypertrophy of calf muscle (Blake, 2002). Eventually patients develop progressive muscle fibre damage, chronic inflammation, and fibrosis (Blake, 2002; Desguerre et al., 2009; Snow et al., 2013). However, in the first two weeks of life, muscle in *mdx* mice is indistinguishable from wild-type (WT) littermates. Mice display early dystrophinopathy-like pathology starting at 3-6 weeks of age (an equivalent of 8-14 human years), when the muscle fibers of the *mdx* mouse undergo focal necrosis and mice have elevated

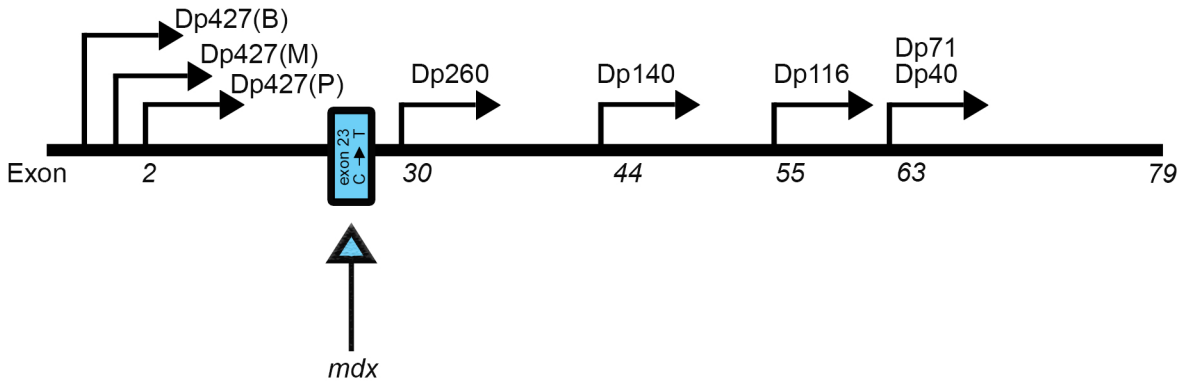

Figure 1 Location of nonsense mutations in exon 23 of DMD gene in the *mdx* mouse model.

serum creatine kinase, pyruvate kinase, and macrophages (Vaillend et al., 1995; McGreevy et al., 2015). Subsequent to this acute degeneration, *mdx* skeletal muscle enters a stable phase, most likely due to robust regeneration wherein muscles becomes hyperplasia and thus appear normal by 10 weeks of age (DiMario et al., 1991). In contrast to the human condition, *mdx* mice do not show the long-term effects of necrosis and regeneration (Miranda et al., 2016), and the *mdx* muscle, instead, shows successful muscle fibre regeneration and reduced endomysial fibrosis (Muntoni et al., 1991; Miranda et al., 2016). As a result, *mdx* mice exhibit the most severe phenotype only after 15 months of age. This includes muscle wasting, scoliosis and heart failure (McGreevy et al., 2015). Unlike DMD patients, adult *mdx* mice before 12 months of age do not show impairments in general mobility (Vaillend et al., 1995). These differences are most likely due to differences in body architecture between mice and men, where mice have greater compensatory mechanisms and regenerative capacity (McGreevy et al., 2015; Remmelink et al., 2016). However, *mdx* mice do show clear functional impairments when tested under strenuous endurance conditions, potentially from reduced muscle regeneration (van Putten et al., 2012; Remmelink et al., 2016).

Impairment in muscle regeneration has been attributed, in part, to impaired asymmetric cell division in satellite cells of *mdx* mice (Dumont et al., 2015). Satellite cells, located between the sarcolemma and basal lamina of myofibers, are the stem cell population of muscle. These cells become proliferative following injury and progeny specify into either a committed myogenic progenitor cell to regenerate muscle, or self-renew to replenish the satellite cell pool (Morgan and Partridge, 2003). Work in the Rudnicki laboratory has demonstrated that this specification is reduced in *mdx* mice (Dumont et al., 2015). In healthy mice, Mark2 (MAP/microtubule affinity-regulating kinase 2, the homolog of Par1 in drosophila) phosphorylates Pard3, signaling for the redistribution of the PAR complex (comprised of Par3, Par6 and atypical protein kinase C) to the

opposite side of the cell (Neumuller and Knoblich, 2009). Redistribution of PAR is required for asymmetric stem cell division, in which one daughter cell specifies to a myogenic progenitor cell and the other daughter cell retains its proliferative ability (figure 2A; Dumont et al., 2015). In the absence of dystrophin in *mdx* mice, there is down-regulation of the serine-threonine kinase Mark2, and the PAR complex becomes uniformly localized around the periphery of the cell in a nonpolarized manner (Dumont et al., 2015). This results in reduced asymmetric division and causes a transient expansion of proliferative satellite cells (satellite cell hyperplasia) as well as a downstream reduction in the number of committed progenitors capable of regenerating muscle (figure 2B; Dumont et al., 2015). Therefore, dystrophin has an essential role in establishing PAR-mediated polarity of satellite cells (Dumont et al., 2015).

While the role of dystrophin in satellite cells is well-studied, it is not known whether dystrophin also contributes to maintaining neural stem and progenitor cell populations in the brain. Only two regions in the adult brain are capable of significant postnatal neurogenesis: the subventricular zone (SVZ) of the lateral ventricles and the subgranular zone (SGZ) of the dentate gyrus (Zhao et al., 2008) Adult neural stem-like cells (ANSCs) can be cultured from these regions *in vitro* using a neurosphere (NSP) assay (Walker and Kempermann, 2014), where cells from these regions are extracted, isolated, and grown in suspension in growth medium under conditions where only ANSCs proliferate to form NSPs and then initiate specification and differentiation (Rahman et al., 2015). As a result, NSPs are heterogenous clusters of cells, the progeny of a single ANSC (also known as type 1 cells) or its immediate transit amplifying type 2 daughter cells, that by time of harvest are in different stages of commitment towards a neuronal or glial phenotype, thus NSPs differ in size, depending on their rate of proliferation, specification, and differentiation

A. Normal Satellite Cell Division

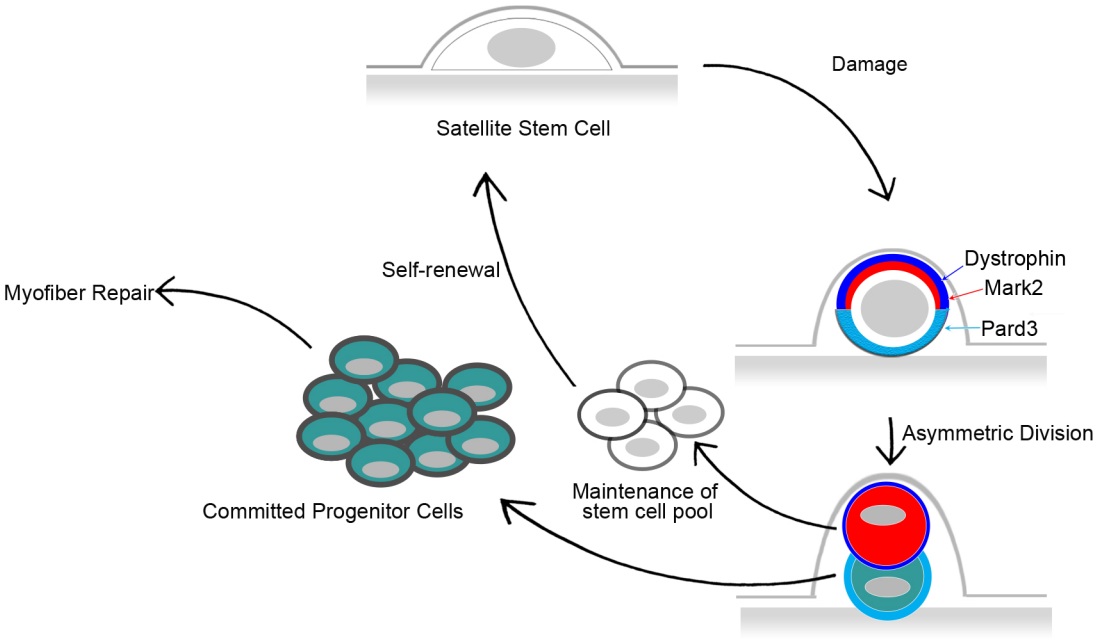

B. *mdx* Satellite Cell Division

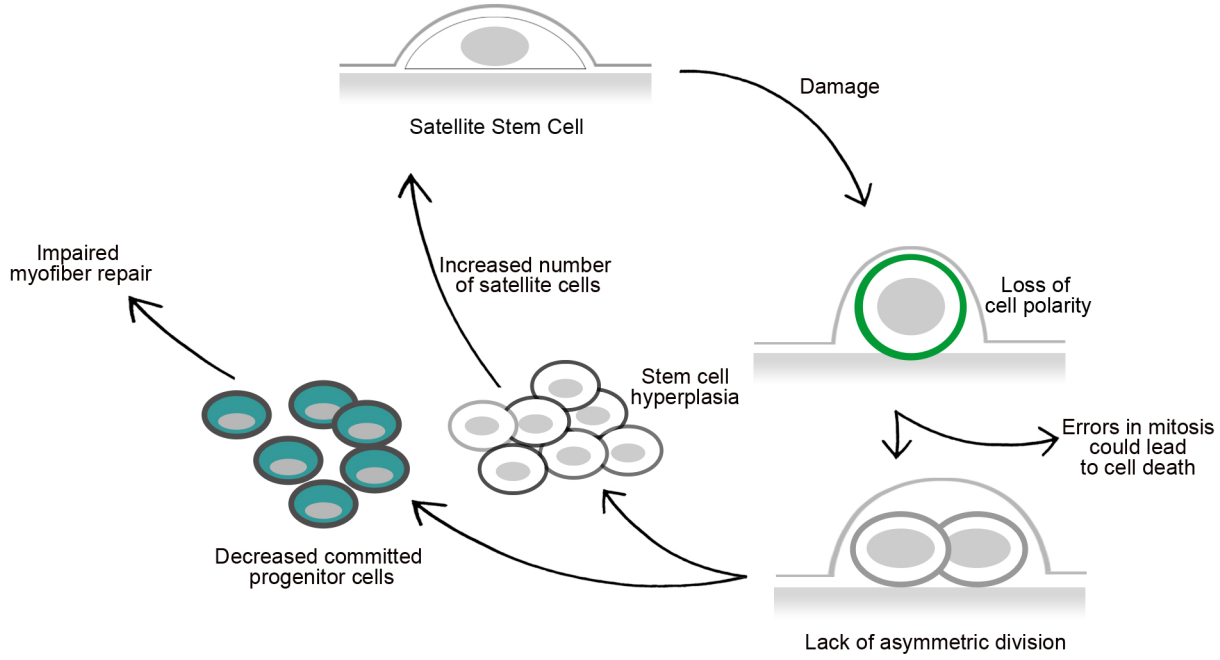

Figure 2 Asymmetric division is impaired in Dp427-deficient satellite cells. (A) In normal satellite cell division, dystrophin interacts with Mark2 which phosphorylates Pard3 causing a redistribution of the Par Complex (Pard3, Pard6 and aPKC) allowing for asymmetric division. (B) In dystrophin deficient satellite cells, Mark2 is downregulated which impairs the ability of the PAR complex to redistribute and results in a loss of polarity, prolonged cell division, reduced number of asymmetrical cell divisions, and a decrease in the number of myogenic progenitor cells. Adapted from Dumont *et al*, 2015.

(Jensen and Parmar, 2006). *In vitro*, *mdx* NSPs from the SVZ are capable of differentiating into neurons, astrocytes and oligodendrocytes like WT (Bond et al., 2015), yet are reduced in size and number compared to WT, suggesting impaired division of ANSCs (Annese et al., 2016). To date, the presence and role of dystrophin in ANSCs in the SGZ is not well understood but a more in-depth analysis may provide insight into the behavioral phenotype of DMD patients. This thesis will to address this research question.

1.1.2 Dystrophin isoforms are differentially deleted in *mdx* mouse models

Since the creation of the *mdx* mouse model, four chemical variants (cv) of the model have been generated: mdx^{2cv}, mdx^{3cv}, mdx^{4cv} and mdx^{5cv} (McGreevy et al., 2015), differentially depleting additional dystrophin isoforms by using different single point mutations along the *DMD* gene (figure 3; Im et al., 1996; McGreevy et al., 2015). All of these models are full body knockouts, each with their own phenotypes (McGreevy et al., 2015). For instance, there is a more intense skeletal phenotype in mdx^{5cv} compared to *mdx* mice, despite both having lost only Dp427, with all other isoforms present (McGreevy et al., 2015). However, to date, there is no animal model devoid of all *DMD* isoforms found in the brain. Again, I sought in this thesis to generate this model.

1.2 One-third of DMD patients are affected by non-progressive cognitive impairments comorbid with neuropsychiatric disorder

Although DMD is thought of as predominantly a muscular disease, one-third of patients are affected by non-progressive cognitive impairments (Vaillend et al., 1995; Hinton et al., 2000). Impairments do not worsen with increasing muscle disease severity, nor age, suggesting cognitive defects are not secondary to muscle degeneration (Snow et al., 2013). Furthermore, DMD patients have a high incidence of neuropsychiatric disorders including: anxiety, attention deficit

A.

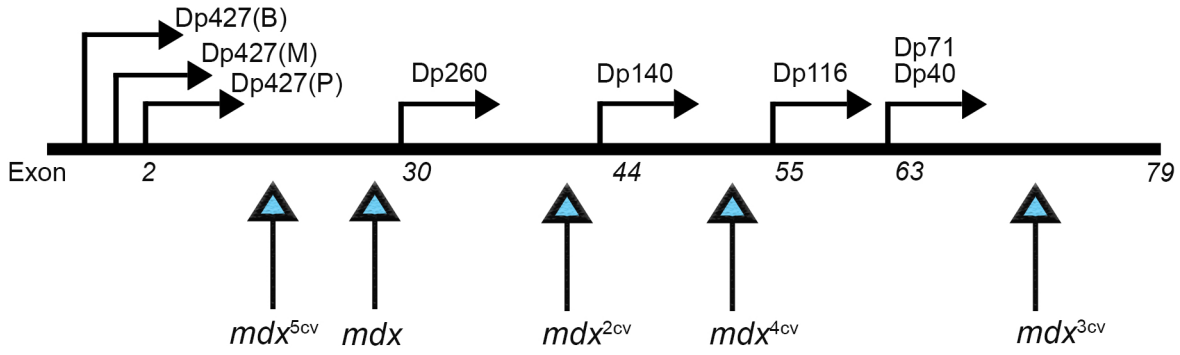

B.

	mdx^{5cv}	*mdx*	*mdx*^{2cv}	*mdx*^{4cv}	*mdx*^{3cv}
Dp427	-	-	-	-	-
Dp260	+	+	-	-	-
Dp140	+	+	+	-	-
Dp116	+	+	+	+	-
Dp71	+	+	+	+	-
Dp40	+	+	+	+	+

Figure 3 Location of mutations in the *DMD* gene in *mdx* mouse model variants. (A) Schematic depicting location of mutations and (B) which isoforms are present.

hyperactivity disorder (ADHD), autism spectrum disorders (ASD), and obsessive-compulsive disorder (OCD; (Bresolin et al., 1994; Mehler, 2000; Hendriksen and Vles, 2008; Snow et al., 2013)).

In the original description of the disease, Duchenne in 1868 described an overall reduction of intellectual abilities in DMD patients (Duchenne, 1868), which has since been reproduced using the Wechsler Intelligence Scale for Children, Wechsler Adult Intelligence Scale, and Stanford-Binet Intelligence Scale (Cotton et al., 2005). The prevalence of intellectual disability in DMD patients is 19% (Hinton et al., 2000), compared to 3% (Cohen et al., 1968; Snow et al., 2013) in the general public . A meta-analytical study conducted by Cotton *et al*, 2005 of data from 32 published papers examining full-scale intelligence quotients (FIQ) of 1224 DMD children and adults established that the mean IQ of DMD patients is 1 standard deviation below the normal population mean (Hinton et al., 2000; Cotton et al., 2005). Importantly, DMD patients also have lower IQ scores when compared to patients who have spinal muscular atrophy (SMA), a different fatally progressive neuromuscular disease (Snow et al., 2013). This provides strong support that motor impairment is not responsible for the cognitive symptoms (Snow et al., 2013). DMD patients also consistently score poorly on tests that assess short-term and working memory (e.g., story memory skills and digit span), deficits in executive functioning (e.g., poor planning skills), and limited verbal comprehension/auditory span, even in patients with apparently normal IQs (Croona et al., 1999; Hinton et al., 2000; Wicksell et al., 2004; Snow et al., 2013).

The prevalence of anxiety in DMD patients is almost twice as high as healthy children of the same age (Banihani et al., 2015). Anxiety is a chronic condition that, when untreated, increases the risk of depression, educational underachievement and substance abuse (Banihani et al., 2015). Unlike the non-progressive cognitive impairment phenotype, anxiety peaks in DMD patients just

before the age when children lose the ability to walk (Bresolin et al., 1994). Approximately 20-27% of DMD patients were diagnosed with an anxiety disorder (Banihani et al., 2015). However, it is important to note that variation exists amongst individual cognitive and behavioural profiles for DMD patients (Hinton et al., 2000; Snow et al., 2013). It is possible that this variance is due to differential profiles of expression of dystrophin isoforms (Hinton et al., 2000; Mehler, 2000), such that the presence of certain isoforms is rescuing the cognitive phenotype (Doorenweerd et al., 2017). Loss of specific isoforms is speculated to increase the severity of the cognitive phenotype, specifically mutations at the 3' end of the gene affecting Dp140 and Dp71, have been associated with lower IQ scores (Cotton et al., 2005; Waite et al., 2009) and mental retardation (Lenk et al., 1993).

Despite these associations, the underlying cause of cognitive disturbances in DMD is unknown. It has been postulated that loss of Dp427 disrupts gamma-aminobutyric acid (GABA) signalling. Dp427 is found in central inhibitory synapses and has a role in anchoring post-synaptic densities (Krasowska et al., 2014). Loss of Dp427 results in a decrease of post-synaptic GABA-$_A$ receptors, altered synaptic transmission, and altered neurexin-neuroligin function (Miranda et al., 2015). As Dp427 recruits neuroligin-2 to post-synaptic densities thereby stabilizing GABA-$_A$ receptor at post-synaptic densities (Krasowska et al., 2014), loss of Dp427 may destabilize GABA-$_A$ receptors resulting in this decrease. Moreover, neurexin and neuroligin, trans-synaptic cell-adhesion molecules (Krasowska et al., 2014) in both excitatory and inhibitory synapses (Blundell et al., 2010) have altered function in the absence of dystrophin (Krasowska et al., 2014). Neuroligins have been implicated in cognitive disorders such as autism (Lise and El-Husseini, 2006) and neurolgin-1 (*NLGN1*; (Blundell et al., 2010)) and neuroligin-2 (*NLGN2*) are candidate genes for mental retardation (Belligni et al., 2012). As well, *B*-dystroglycan, a component of the DAPC as

well as a neurexin ligand, localizes dystrophin at GABA-$_A$ receptors, and assists in synapse formation (Krasowska et al., 2014). Taken together, these implicates the loss of dystrophin and the disruption of associated complexes in enhancing risk for autism spectrum disorders (Miranda et al., 2015). Given the non-progressive nature of these symptoms, disruption may occur during brain development.

Clearly a better understanding of the role of dystrophin, both Dp427 and the smaller isoforms in the brain, and their relationship to cognitive function remains is essential to improve quality of life for DMD patients. Consistent throughout literature, school aged-children with impaired cognitive functioning have reduced academic performance, and this is known to negatively affect self-esteem and self-confidence (Snow et al., 2013). These issues are compounded by existing medical treatment for DMD, since the golden-standard treatment for DMD patients to delay the muscular progression of the disease is steroids. One of the main reasons for discontinuing this treatment, however, is the negative effects on mood and behavioural side effects (Snow et al., 2013), enhancing existing DMD cognitive symptoms. Thus, it is critical to evaluate the roles of these proteins and their effects on cognitive impairments to understand the neuropsychological and neurobehavioural consequences of DMD to assist patients and their families (Snow et al., 2013).

1.2.1 The cognitive phenotype of the *mdx* mouse model is unclear

Behavioural indices of cognitive defects have been reported in *mdx* mice. These include anxiety, autism-related behaviours, learning and memory, and motoric impairment. However, these findings in the literature are inconsistent and challenging to interpret. Below, I review these inconsistencies.

Common tests used to assess anxiety in mice are the light-dark box (LDB), open field (OF), and elevated plus maze (EPM). Each paradigm presents mice with a conflict, for instance in the OF test, mice are conflicted between their desire to explore an open space and their aversion to bright lights (Crawley, 2000). In general, anxiety tests are based on the assumption that highly anxious mice will exhibit less exploratory behaviour (Crawley, 2007). Vaillend *et al*, 1995 concluded that there were no significant differences between WT and *mdx* in time spent in the light compartment nor in the number of transitions from the light to the dark compartment in LDB. In contrast, Remmelink *et al*, 2016 showed *mdx* mice spent significantly less time in the light, with fewer transitions to the light compartment in the LDB. A possible explanation may be sex differences in the *mdx* manifestation of cognitive impairment, as Remmelink *et al*, 2016 used female mice who were homozygous for the *DMD* mutation, whereas Vaillend *et al*, 1995 used hemizygous male mice. Several mouse models, such the TgCRND8 mouse model of Alzheimer's disease (Granger et al., 2016), have been shown to be sexually dimorphic. I argue that because DMD affects primarily males, male mice should be the preferred model. Research using other tests to measure anxiety include EPM (Sekiguchi et al., 2009) and OF (Manning et al., 2014; Remmelink et al., 2016) have both concluded *mdx* mice do not exhibit an anxious phenotype in these paradigms.

The association between DMD and ASD is unclear, with only one publication that has examined behavioural indices of autistic-like traits in the *mdx* mouse model. ASD can encompass three behavioural symptoms: communication deficits, restrictive and repetitive behaviours, and social communication/interaction disorders (Angoa-Perez et al., 2013). Miranda *et al*, 2015 used a battery of behavioural tests to demonstrate that *mdx* mice are socially impaired. Their results were, however, ambiguous. They found no behavioural differences between WT and *mdx* mice in the

three-chamber sociability test (preference for unfamiliar individual rather than an object) or social novelty (preference for unfamiliar mouse rather than a familiar mouse (Miranda et al., 2015), two tests where mice do not directly interact. When an intruder was introduced to the home cage of *mdx* mice, *mdx* mice had fewer interactions with the intruding mouse regardless of sex (Miranda et al., 2015). Additionally, when introduced to both a new mouse and a new environment, *mdx* mice exhibited increased freezing behaviours and reduced interactions with intruders than WT (Miranda et al., 2015). Therefore, a loss of Dp427 in *mdx* mice did not appear to affect the processing of socially relevant behaviour but did impair adaptive behaviours underling interaction with intruding mice (Miranda et al., 2015). The authors suggested *mdx* mice may have enhanced fear-related responses that contribute to these social deficits (Miranda 2015). Based on these findings, I chose, in this thesis, to test directly whether fear-related learning is altered in *mdx* mice.

Fear learning has been previously assessed but discrepancies in the literature regarding the behavioural response of *mdx* mice suggests additional studies are required (Sekiguchi et al., 2009; Chaussenot et al., 2015; Miranda et al., 2015). In the passive avoidance test, mice learn to avoid the location where they had previously received a foot shock. Here, memory performance is positively correlated to latency to enter the associated compartment (Muntoni et al., 1991). Muntoni *et al,* 1991 found *mdx* mice re-entered the shock compartment quicker than WT mice, concluding *mdx* mice had a reduced capacity to make these associations and retain the learned information. Fear learning is also tested using the contextual fear conditioning (FC) task that requires a mouse to learn and remember an association between an aversive stimulus (shock) and either a cue (tone) or the testing atmosphere (context; Crawley, 2000). In response to one tone-shock pairing, Sekiguchi et al found that *mdx* mice had a heightened response (more freezing behaviour), as well as when the mice were returned to the testing chamber 24-hours later,

concluding that *mdx* mice had enhanced fear-motivated conditioned defensive response (Sekiguchi et al., 2009). This, however, directly contradicts from (Chaussenot et al., 2015) , where *mdx* mice had reduced acquisition rates to multiple tone-shock pairings and were unable to retain these associations when re-introduced to the same cue in a different testing environment 24 hours after the acquisition trial (Chaussenot et al., 2015). One key difference between these studies is the number of tone-shock pairings mice received during the acquisition trial. Sekiguchi *et al* 2009 used a single trial with 1 tone-shock pairing, whereas Chaussenot *et al* 2015 tested using either one or two acquisition trials consisting of 5 tone-shock pairings. The tone-shock association is expected to strengthen with increased number tone-shock pairings (Crawley, 2007). It has been established that *mdx* mice respond to foot shock of equal intensity the same as WT, thus physical sensitivity to pain is not the cause for these phenotypic differences (Chaussenot et al., 2015).

Spatial learning and memory has also been investigated in the *mdx* mice. This hippocampal-dependent function has been assessed by radial arm maze (Vaillend et al., 1998; Chaussenot et al., 2015), Barnes maze (Remmelink et al., 2016), T-maze (Vaillend et al., 1995; Remmelink et al., 2016), and Morris Water Maze (MWM; (Sesay et al., 1996; Vaillend et al., 2004; Chaussenot et al., 2015)). In the T-maze, Vaillend *et al*, 1995 showed that *mdx* mice exhibit lower performance during retention sessions, suggesting impaired long-term learning and memory consolidation (Vaillend et al., 1995). By contrast, using the MWM Sesay *et al,* 1996 observed no differences in escape latency during training days nor reversal days, concluding that spatial learning and memory was unaffected by loss of Dp427.

There are also limited behavioral studies using the variant *mdx* mouse models. It is expected that smaller dystrophin isoforms may ameliorate the cognitive phenotypes seen of *mdx* mice thus variant mice should show more consistent or more exacerbated behavioural indices of cognitive

impairment (Lenk et al., 1993; Sesay et al., 1996). This is supported by Vaillend (1998) using *mdx*^{3cv} mice, in which all dystrophin isoforms (Dp427, Dp260, Dp140, Dp116 and Dp71) are depleted except for Dp40. Surprisingly, these mice did not show any spatial memory deficits in the radial arm maze, whereas *mdx* mice did (Vaillend et al., 1998).

Taken together, DMD is more than just a muscle phenotype – there is substantial evidence pointing to CNS involvement in the disease (Snow et al., 2013). Loss of embryonic dystrophin results in physical changes to brain structures involved in cognition, and consequential behavioural impairments. Yet, despite all DMD patients being devoid of Dp427, only one-third are affected by non-progressive cognitive impairments. Assessing the mechanism of these impairments using the *mdx* and *mdx* variant mouse models have been inconclusive. I hypothesize that this variation in reported cognitive phenotypes could be either a) the use of unoptimized (or different) behavioural paradigms targeting *mdx* mouse cognition, or b) the presence of smaller dystrophin isoforms in the brain that rescue cognition. Thus, a mouse model that completely rids the brain of all dystrophin isoforms, Dp427, Dp260, Dp140, Dp116, Dp71 and Dp40, would prove to be invaluable.

Table 3 Summary of behavioural tests completed on mdx mouse model

Behaviour	Author(s), Year	Behavioural Test	*n*, sex, genotype, age
Anxiety	Manning et al, 2014	Open Field	?, m, C57Bl/10ScSn-mdx, 6 wks ?, m, C57Bl/10ScSn-WT, 6 wks
	Remmelink et al, 2016	Light-Dark Box	13, f, C57Bl/6ScSn-mdx, 21 wks 11, f, C57Bl/6ScSn-WT, 21 wks
	Remmelink et al, 2016	Open Field	13, f, C57Bl/6ScSn-mdx, 21 wks 11, f, C57Bl/6ScSn-WT, 21 wks
	Sekiguchi et al, 2009	Elevated Plus Maze	11, m, C57Bl/10J-mdx, 16 wks 15, m, C57Bl/10J-WT, 16 wks
	Vaillend et al, 1995	Light Dark Box	25, m, C57Bl/10ScSn-mdx, 11 wks 23, m, C57Bl/10ScSn-B10, 11 wks
Autism-Related Behaviours	Miranda et al, 2015	3-Chamber Sociability	13, m, C57Bl/10ScSn-mdx, 21 wks 10, m, C57Bl/10ScSn-B10, 21 wks
	Miranda et al, 2015	Female-Male Social Interaction	13, m, C57Bl/10ScSn-mdx, 21 wks 10, m, C57Bl/10ScSn-B10, 21 wks
		Male-Male Social Interaction	13, m, C57Bl/10ScSn-mdx, 21 wks 10, m, C57Bl/10ScSn-B10, 21 wks
	Miranda et al, 2015	Male Exposure to Anesthetized Female	13, m, C57Bl/10ScSn-mdx, 21 wks 10, m, C57Bl/10ScSn-B10, 21 wks
	Miranda et al, 2015	Resident Intruder Test	15, m, C57Bl/10ScSn-mdx, 20 wks 15, m, C57Bl/10ScSn-B10, 20 wks
Learning and Memory	Chaussenot et al, 2015	Acoustic Startle Response	?, m, C57Bl/10ScSn-mdx/J, 10-16 wks ?, m, C57Bl/10ScSnOlaHsd, 10-16 wks
	Chaussenot et al, 2015	Fear Conditioning	?, m, C57Bl/10ScSn-mdx/J, 10-16 wks ?, m, C57Bl/10ScSnOlaHsd, 10-16 wks
	Chaussenot et al, 2015	Morris Water Maze	?, m, C57Bl/10ScSn-mdx/J, 10-16 wks ?, m, C57Bl/10ScSnOlaHsd, 10-16 wks
	Chaussenot et al, 2015	Radial Maze	?, m, C57Bl/10ScSn-mdx/J, 10-16 wks ?, m, C57Bl/10ScSnOlaHsd, 10-16 wks
	Lewon et al, 2017	Operant Conditioning with food reward	6, m, C57Bl/10ScSn-mdx/J, 13.5-35 wks 6, m, C57Bl/10ScSn, 13.5-35 wks
	Lewon et al, 2017	Avoidance Task	6, m, C57Bl/10ScSn-mdx, 13.5-35 wks 6, m, C57Bl/10ScSn-WT, 13.5-35 wks
	Mutoni et al, 1991	Passive Avoidance Test	10, f, C57Bl/6ScSn-mdx, 16-22 wks 9, f, C57Bl/6ScSn-WT, 16-22 wks
	Remmelink et al, 2016	Barnes Maze	13, f, C57Bl/6ScSn-mdx, 21 wks 11, f, C57Bl/6ScSn-WT, 21 wks
	Remmelink et al, 2016	DL/RL Home Cage Task	13, f, C57Bl/6ScSn-mdx, 21 wks 11, f, C57Bl/6ScSn-WT, 21 wks
	Remmelink et al, 2016	Home-cage Avoidance Learning Task	13, f, C57Bl/6ScSn-mdx, 21 wks 11, f, C57Bl/6ScSn-WT, 21 wks
	Remmelink et al, 2016	T-Maze	13, f, C57Bl/6ScSn-mdx, 21 wks 11, f, C57Bl/6ScSn-WT, 21 wks
	Sekiguchi et al, 2009	Electrical Foot shock (contextual memory)	9, C57Bl/10J-mdx, 13-17 wks 10, C57Bl/10J-WT, 13-17 wks
	Sesay et al, 1996	Morris Water Maze	8, ?, C57Bl/10-mdx, ? 8, ?, C57Bl/10-WT, ?
	Vaillened et al, 1995	Positively Reinforced Operant Learning Task	25, m, C57Bl/10ScSn-mdx, 11 wks 21, m, C57Bl/10ScSn-B10, 11 wks
	Vaillend et al, 1995	T-maze (with 6 h or 24 h retention interval)	25 (6 h)/24 (24 h), m, C57Bl/10ScSn-mdx, 11 wks 23 (6 h)/21 (24 h), m, C57Bl/10ScSn-B10, 11 wks
	Vaillend et al, 1998	(Spatial Discrimination) Radial Maze	13, m, C57Bl/10ScSn-mdx, 11 wks 13, m, C57Bl/10ScSn-B10, 11 wks 10, m, C57Bl/6Ros, 11 wks 14, m, C57Bl/6Ros-mdx3cv, 11 wks
	Vaillend et al, 2004	Morris Water Maze	22, m, C57Bl/10ScSn-mdx, 10 wks 25, m, C57Bl/10ScSn-B10, 10 wks
	Vaillend et al, 2004	Object Recognition in Open Field	14, m, C57Bl/10ScSn-mdx, 12-20 wks 12, m, C57Bl/10ScSn-B10, 12-20 wks
Spontaneous Motor Activity	Mutoni et al, 1991	Beam Break	15, f, C57Bl/6ScSn-mdx, 16-22 wks 10, f, C57Bl/6ScSn-WT, 16-22 wks
Motoric Impairments	Prigogine et al, 2012	Rotarod, Catwalk Runway, Wire Tests	?, ?, C57Bl/10ScSn-mdx, ? ?, ?, C57Bl/10ScSn-WT, ?
	Vaillend et al, 1995	Spontaneous Locomotor Activity	25, m, C57Bl/10ScSn-mdx, 11 wks 23, m, C57Bl/10ScSn-B10, 11 wks
Emotional Test	Sekiguchi et al, 2009	Restraint Test	17, C57Bl/10J-mdx, 16-17 wks 18, C57Bl/10J-WT, 16-17 wks
Reflex Test	Vaillend et al, 1995	Traction Reflex Test	25, m, C57Bl/10ScSn-mdx, 11 wks 23, m, C57Bl/10ScSn-B10, 11 wks

1.3 Objectives and Hypothesis

The overarching objective of this thesis was to establish whether the loss of Dp427 and *DMD* isoforms expressed in hippocampus disrupt hippocampal neurogenesis thereby altering behavioural indices of anxiety, stereotypies, and/or learning and memory. I hypothesized that the loss of Dp427 in ANSCs of the SGZ would disrupt the balance between asymmetric and symmetric division as previously shown in muscle satellite cells (Dumont et al., 2015). I further hypothesized that this defect would be exacerbated in a new brain-specific mouse model devoid of all *DMD* isoforms resulting in anxiety, autism-related behavior and learning and memory deficits.

To test these hypotheses, I proposed three specific aims:

(1) Assess whether Dp427 is expressed by hippocampal nestin-positive type 1 (ANSC) and 2a neural progenitor cells (the transit amplifying immediate progeny of ANSCs) and establish whether deletion of Dp427 is sufficient to disrupt symmetric and asymmetric cell division *in vitro*.

(2) Establish whether loss of Dp427 in adult hippocampus is sufficient to alter behavioral indices of anxiety, autism-related behavior and learning and memory in *mdx* mice.

(3) Generate brain-specific conditional dystrophin knockout mouse models where dystrophin is depleted (a) embryonically from all nestin-expressing cells and (b) postnatally from type 1 and 2a ANSC and neural progenitor cells.

2 MATERIALS AND METHODS

2.1 Animal Experimentation

Wild-type (WT) C57Bl/10ScSn/J mice (CAT # JAX#000476, n = 12) and dmd^{mdx} (*mdx*) mice (CAT# JAX#001801, n = 13) were obtained from Jackson Laboratories. At total of 2 mice (n=1 WT and n=1 *mdx* were used for Western blotting as described below. The remaining mice

were assessed behaviourally as described below. For neurosphere cultures, pups from WT and *mdx* breeding were obtained as described below. Mice were maintained on a 12:12 light:dark cycle with zeitgeber (ZT) 0 set to 7:00 am. Mice had *ad libitum* access to food and water. Mice were group housed upon weaning, and individually housed at 10 weeks ± 2 weeks of age until sacrifice. A total of *n*=11 male WT and *n*=12 male *mdx* mice were used for behavioural analysis in this study. Genotyping was confirmed at the time of weaning and again at time of sacrifice. PCR amplification was performed on a Whatman Biometra TGradient96 system. DNA that was isolated from tail snips, was amplified using primers and cycling parameters found in table 1.2. All protocols and experiments were approved by the Animal Care Committee of the University of Ottawa and performed according to guidelines set forth by the Canadian Council on Animal Care.

Animals undergoing behavioral assessments were sacrificed eight days after completion of all behavioral tests. Mice were anesthetized with 0.155 cc of 65 mg/ml euthanyl (Bimeda-MTC Animal Health Ins., 1EUS001) via intraperitoneal (i.p.) injection and euthanized by cardiac perfusion or decapitation once fully anesthetized. For cardiac perfusion, their hearts were exposed, the right atrium bisected, and exsanguinated using 20 mL of 10 mM phosphate buffered saline (PBS; 10 mM phosphate, 154 mM NaCl) injected into the right ventricle with a 23 ¾ gauge butterfly needle (BD Vacutainer Safety-Lok, #367292). Mice were then perfused with 20 mL of 4% paraformaldehyde (PFA; Sigma Aldrich, # F1635) (96% 10mM PBS). Brains and tibialis anterior (TA) muscle were removed and stored at 4°C overnight in 15 mL falcon tubes containing 10 mL of 4% PFA. The following day, this solution was replaced with 20% sucrose in 10mM PBS containing 0.001% sodium azide. For protein assessments, brain and tibialis anterior muscle were collected without perfusion. Brains were placed in a petri dish containing ice-cold PBS and

Table 4 Genotyping protocols

Gene	*Reaction Conditions*	*Cycling & Amplicon Sizes*
fDMDH $^{f/Y}$	fDMDHF:5'-GACCCTCCCGCCTTTGTCTTTTGAGTGTCG-3' fDMDHR: 5'-TTTGGGGTGGAGGCTGTCACTGTGTTACAT-3' Primer concentrations: 50 pmol/µl	95°C 2 min 40 cycles 95°C 5 s 65°C 90s (+allele=451 bp) (-allele=604 bp)
Gt(ROSA)26 EYFP	Gt(ROSA)26 YFPF:5'-GCGAAGAGTTTGTCCTCAACC-3' Gt(ROSA)26 YFPR1: 5'-GGA GCG GGA GAA ATG GAT ATG-3' Gt(ROSA)26 YFPR2: 5'-AAA GTC GCT CTG AGT TGT TAT-3' Primer concentrations: F: 5 µM, R: 2.5 µM	94°C 5 min 35 cycles 94°C 5 s 66°C 35s 72°C 60s 72°C 5 min (+allele=330 bp) (-allele=250 bp)
NestinCre	CreF: 5'-ATTTGCCTGCATTACCGGTC-3' CreR: 5'-ATCAACGTTTTGTTTTCGGA-3' Primer concentrations: 100 ng/ml	94°C 5 min 30 cycles 94°C 30 s 56°C 30s 72°C 60s (+allele=350 bp)
NestinCreER $^{T2\text{-}IRES\text{-}hPLAP}$	CreERT2(SB)F: 5'-TTGCCCCTGTTTCACTATCCAG-3' CreERT2(SB)R: 5'-TGCTGTTTCACTGGTTATGCGG-3' Primer concentrations: 10 pmol/µl	94°C 3 min 32 cycles 94°C 30 s 62.2°C 60s 72°C 60s 72°C 5 min (+allele=700 bp)
Gt(ROSA)26mT/mG	Gt(ROSA)26mT/mGF1: 5'-CTCTGCTGCCTCCTGGCTTCT-3' Gt(ROSA)26mT/mGF2: 5'-CGAGGCGGATCACAAGCAATA-3' Gt(ROSA)26mT/mGR: 5'-TCAATGGGCGGGGGTCGTT-3' Primer concentrations: 20 pmol/µl	94°C 3 min 35 cycles 94°C 30 s 71°C 60s 72°C 60s 72°C 2 min (+allele=300 bp) (-allele=250 bp)
NestinCreER $^{T2\text{-}5.1}$	CreERT2F: 5'- ATTTGCCTGCATTACCGGTC-3' CreERT2R: 5'- ATCAACGTT TTCTTTTCGG-3' Primer concentrations: 10 pmol/µl	94°C 60 s 36 cycles 94°C 30 s 53°C 30s 72°C 60s 72°C 10 min (+allele=350 bp)

the hippocampus, temporal cortex, and cerebellum were dissected, flash-frozen in liquid nitrogen, and stored at -80°C until protein processing.

2.2 Development of transgenic mouse lines

Two inducible tissue-specific DMD knockout mouse lines and one constitutive tissue specific DMD knockout line were developed. NestinCre^{ERT2} (5.1) transgenics, generously provided by Dr. Ryiochiro Kageyama in collaboration with Dr. Diane Lagace (Imayoshi et al., 2006) were crossed to double-fluorescent tandom dimer Tomato (mT)/membrane targeted green fluorescent reporter (mG) reporter mice [B6.129(Cg)-Gt(ROSA)26Sortm4(ACTB-tdTomato,-EGFP)Luo/J (referred to as R26R mT/mG; Jackson stock# 007676; (Muzumdar et al., 2007)). Mice were then bred to female fDMDH$^{f/f}$ mice (unpublished) kindly provided by Dr. Michael Rudnicki in collaboration with Dr. Kevin Campbell, University of Iowa. The breeding scheme is depicted in figure 4. We further crossed NestinCre^{ERT2} (SB) (Cicero et al., 2009) generously provided by Dr. Suzanne Baker in collaboration with Dr. Ruth Slack and Dr. Steffany Bennett already placed on a Gt(ROSA)26Sortm1(EYFP)Cos/J background (referred to as R26R YFP; Jackson stock# 006148) to fDMDH$^{f/f}$ mice. Figure 5 depicts this breeding scheme. In both lines, recombination was induced using tamoxifen (TAM, Sigma-Aldrich, CAT# T5648) administered at 180 mg/kg/day with an injection schedule of 1 injection per day for 3 days. TAM was dissolved in 10% EtOH/90% sunflower oil. Mice were sacrificed 24 hours following the last TAM injection.

Constitutive knockout mice were generated by breeding fDMDH$^{f/f}$ female mice to NestinCre^{+} mice provided by Dr. Ruth Slack (Berube et al., 2005). The breeding scheme is depicted in figure 6. To confirm the specificity of the NestinCre promoter, an additional mouse

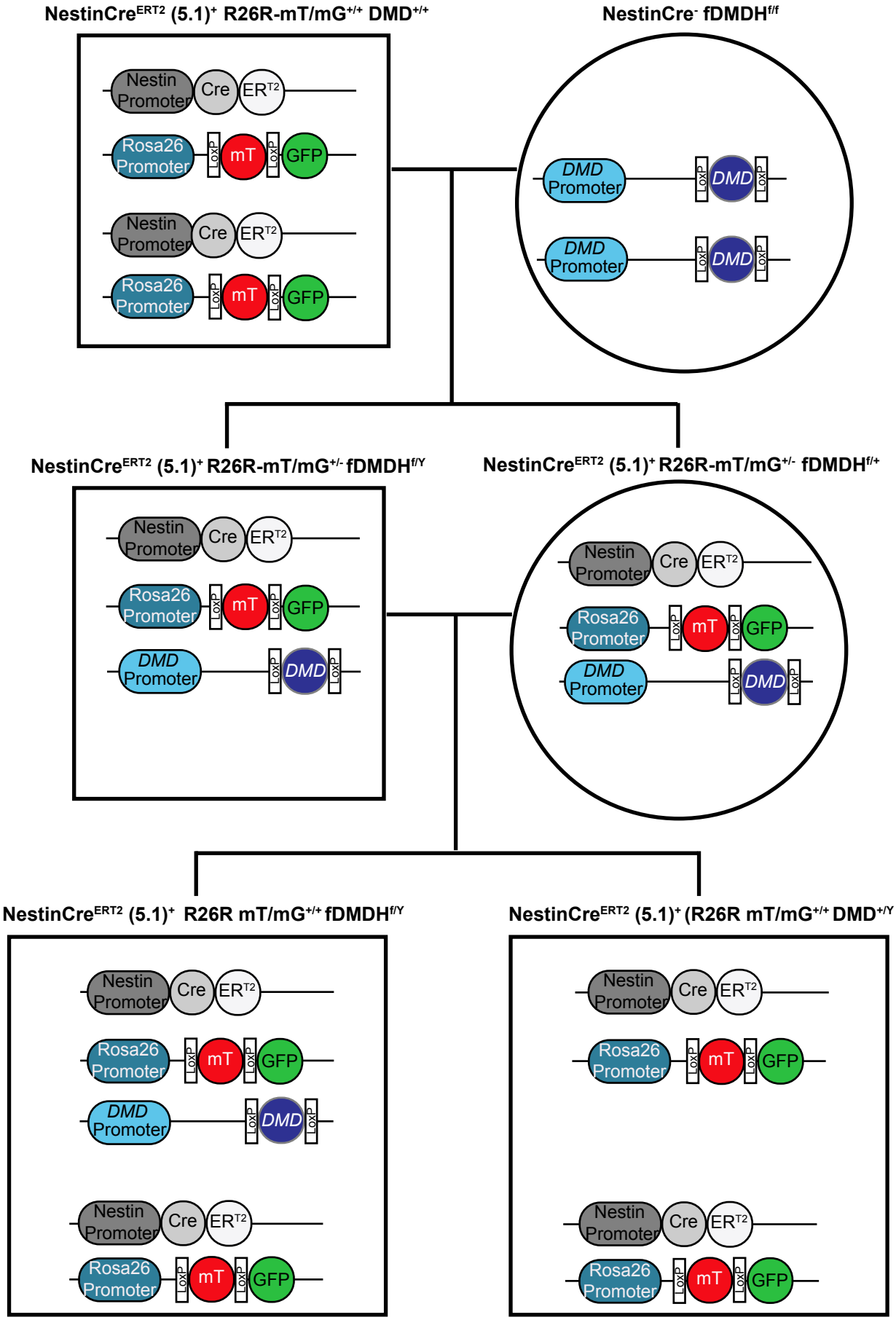

Figure 4 Breeding scheme for the generation of a nestin Cre^{ERT2}-inducible brain-specific *DMD* knock-out mouse model on a mT/mG reporter line

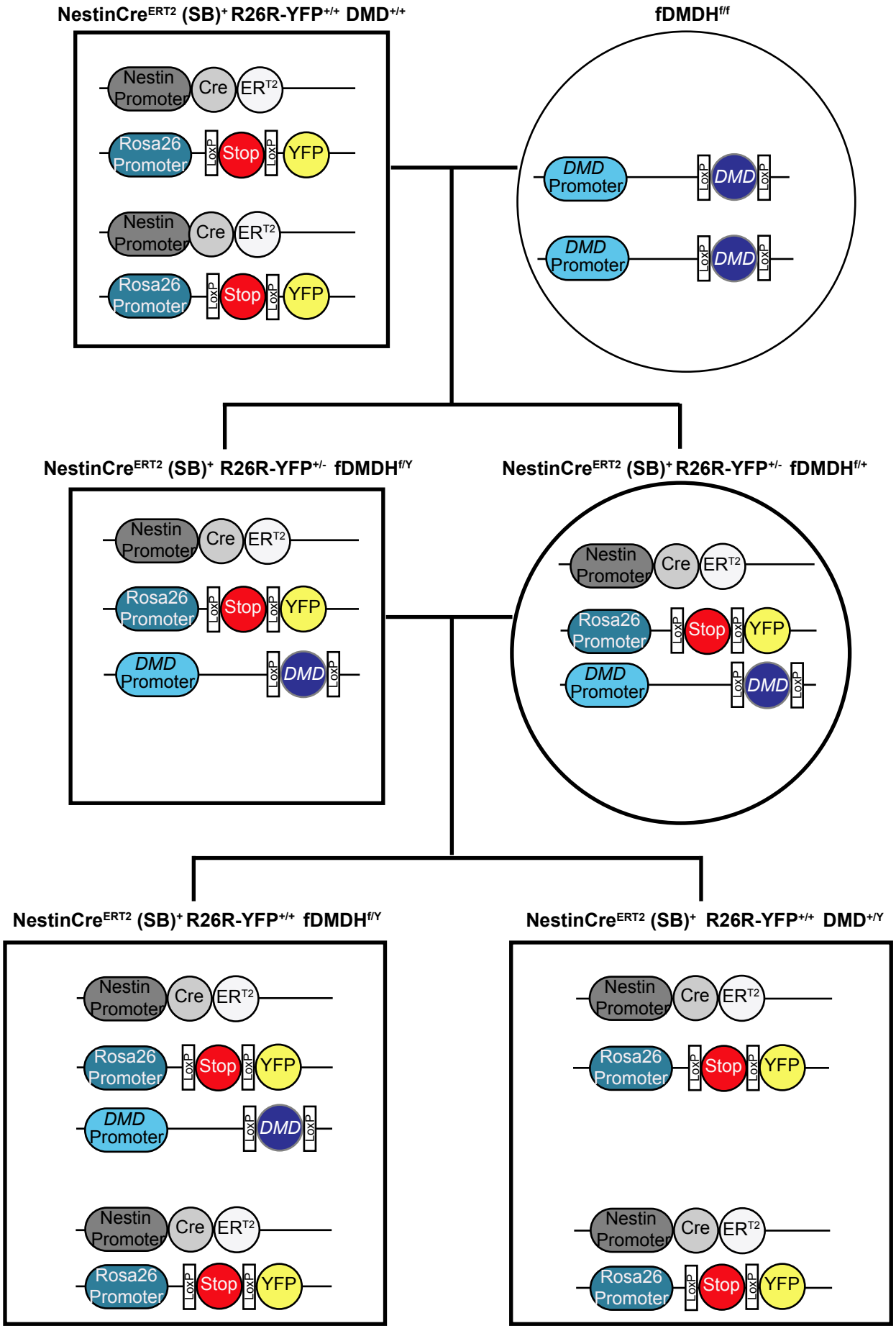

Figure 5 Breeding scheme for the generation of a nestin Cre^{ERT2}-inducible brain-specific *DMD* knock-out mouse model on a YFP reporter line.

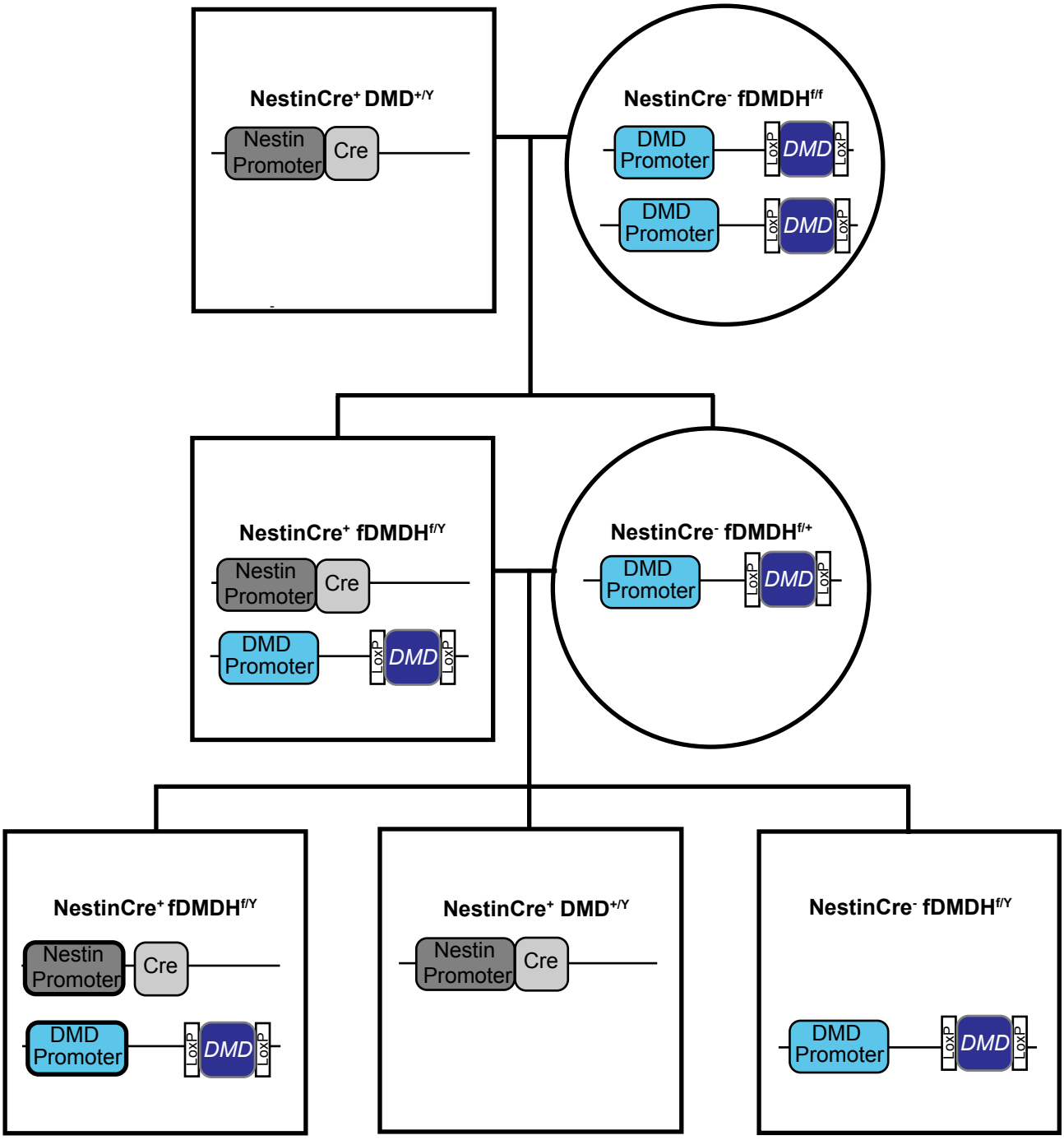

Figure 6 Breeding scheme for the generation of a constitutive brain-specific dystrophin knock-out mouse model.

model was generated by placing NestinCre^{+} mice on the mT/mG reporter line (Muzumdar et al., 2007).

2.3 Tissue Sectioning

Following cryoprotection, brains were coronally sectioned in 30 μm sections using a Leica CM1900 Cryostat at -20°C. Eight serial sets comprising the hippocampus and dentate gyrus (bregma -1.1 to -3.5 μm) were collected in ten serial wells (Greiner Bio-One, #203-170) containing 0.1% NaN3 in 10 mM PBS and stored at 4°C until processed for free-floating immunofluorescence.

2.4 Immunofluorescence and Confocal Microscopy (IFC)

For staining in brain, one series of ten sections (bregma matched from -1.1 to -3.5 μm) per mouse line were washed with 10 mM PBS for 5 minutes, incubated in primary antibody (1/2000 rabbit anti-GFP; Abcam, # ab290) diluted in Antibody Buffer (3% BSA, 0.3% Triton-X in 10 mM PBS) overnight at 4°C. The following day, the sections were washed 3 x for 5 minutes in 10 mM PBS at room temperature before incubation with secondary antibody (1/100 FITC donkey anti-rabbit IgG; Jackson Immuno, # 711-096-152) for 1 h at room temperature on a Belly Dancer shaker (Stovall Life Science, 115V - BDRAA115S, # 01062) set to medium speed. Sections were washed 3 x 5 minutes in 10 mM PBS, and mounted onto microscope slides (Superfrost/Plus, Fisherbrand CAT#), using antifade reagent (ProLong Gold, # P36930) and covered with #1.5 microscope cover glass (Fisherbrand, #125441G). Sections were imaged by confocal laser scanning microscopy using a Leica TCS SP5, Leica Microsystems.

IFC of TA muscle was provided by Dr. Caro Brun, postdoctoral fellow in Dr. Michael Rudnicki's lab. TA muscles were isolated, fixed in 0.1% PFA overnight, and successively

transferred into 10%, 20% and 30% sucrose. Muscle cross-sections (10 μm) were obtained using a cryostat, and sections were permeabilized for 10 minutes in 0.1% Triton X-100, 0.1M Glycine in PBS at room temperature. Sections were then blocked with a blocking solution of 5% goat serum, 2% BSA, with 1/40 M.O.M blocking reagent (Vector Laboratories) in PBS for 1h at RT. Sections were incubated in primary antibody (1/2 mouse anti-Pax7; Developmental Studies Hybridoma Bank, AB_528428; 1/1000 chicken anti-GFP; Abcam, #ab13970), and blocking buffer overnight at 4°C. The following day, sections were washed 3 times in PBS, and labelled with secondary antibodies (1/1000 Alexa488 goat anti-chicken; Life Technologies, A – 11039; 1/1000 Alexa647 donkey anti-mouse; Life Technologies, A – 31571) and incubated in blocking buffer for 1 h at room temperature. Sections were washed in 3 times in PBS, and Hoechst (1/1000 in PBS, #33342) was used as a nuclear counterstain. Slides were rinsed once more with PBS and mounted with Permafluor (Fisher). Immunostaining was imaged using Axio Observer.Z1 microscope equipped with a LSM510 META confocal laser scanner.

2.5 Neurosphere Assay

All chemical reagents were obtained from Sigma-Aldrich (St. Louis, MO, USA) and all cell culture reagents were obtained from Invitrogen (Burlington, ON, Canada) unless otherwise stated. ANSCs and type 2a neural progenitor cells were cultured as described in (Imbeault et al., 2009) with some modifications. Briefly, cells were isolated from the hippocampi of postnatal day 0 - 3 (P0-P3) of WT and *mdx* pups. Animals were sacrificed by lethal injection with euthanyl (Bimeda-MTC Animal Health Ins., 1EUS001) and decapitated. Under a Leica MZ6 dissecting microscope, hippocampi were removed and dissected free of blood vessels and choroid plexus. Hippocampi were minced with a scalpel in ice-cold artificial cerebrospinal fluid (ACSF: 26 mM

$NaHCO_3$, 124 mM NaCl, 5 mM KCl, 2 mM $CaCl_2$, 1.3 mM $MgCl_2$, 10 mM D-glucose, 100 U/mL penicillin, and 100 µg/mL streptomycin) transferred to a 15 mL Falcon tube and enzymatically dissociated in 0.1 mM $CaCl_2$, 3.2 mM $MgCl_2$, 10 mM D-glucose, 1% penicillin/streptomycin, 0.1 mg/ml papain (Sigma-Aldrich P-4762), 80 µg/ml Dispase 1 (Sigma-Aldrich D4818) and 10 mg/ml DNase I (Roche 11 284932001) for 1 h at 37°C. Hippocampi from $n = 3$ pups per genotype were pooled for each culture. Ten mL of PBS was added, and samples were centrifuged at 300 x g for 15 mins. The pellets were resuspended, triturated in 5 mL of PBS using a sterile pipette, and collected by centrifugation at 300 x g for 5 min. Single cells were resuspended in maintenance media (Dulbecco's modified Eagle's medium/F12; DMEM/F12, Invitrogen #12400-024) 2 mM L-glutamine (ThermoFisher Scientific, #A2916801), 100 U/ml penicillin, 100 µg/ml streptomycin, 1X B27 supplement (ThermoFisher Scientific, #17504044), 20 ng/ml human recombinant epidermal growth factor (EGF, ThermoFisher Scientific, #PHG0311), and 10 ng/ml basic fibroblast growth factor (FGF-2, ThermoFisher Scientific, #13256029) in 60 mm Petri dishes (Fisher Scientific, Nepean, ON, Canada).

Cell viability was assessed by Trypan Blue (ThermoFisher, #15250061) and counted with a hemocytometer. Cells were plated at a density of 1.1 x 10^5 viable cells/well in Corning Ultra-Low Attachment Surface 6-well plates (CAT#3471). A total of 6 wells were plated per culture. Cultures were maintained at 37°C in a 5% CO_2 atmosphere, and plates were tapped twice per day beginning on days *in vitr*o (DIV) 1. On DIV 2, 2 mL of fresh maintenance media and growth factor mix was added to each well. On DIV 4, 6 and 8, 2 mL of media was removed from each well and replaced with two mL of fresh maintenance media and growth factor mix. Cultures were imaged on DIV 9 using a Leica DM IL inverted microscope with a Q-Imaging Qicam FAST 1397 camera. Entire wells were imaged in serial photomicrographs to assess number and size of neurospheres

per well. Following imaging, cultures were pelleted by centrifugation and each well was dissociated into separate single cell suspensions in 1x Trypsin (Promega, #V5111). Cell number was established by Trypan Blue hemocytometer counts. A total of 1.1 x 10^5 viable cells/well were re-plated in Corning Ultra-Low Attachment Surface 6-well plates. Secondary neurospheres were cultured identically to primary cultures. On DIV 9, every neurosphere in each well was imaged, and cell numbers per well established as described above. For all analyses, neurosphere numbers and area were determined using ImageJ-FX software with Fiji plugin (National Institute of Health).

2.6 Western Blot

Hippocampi and tibialis anterior muscle were dissected from *n*=1 WT (C57Bl/10ScSn/J) and *n*=1 *mdx* mouse at 2 months of age. Western blotting was performed by Dr. Stephanie Fowler as described in (Fowler et al., 2013). Briefly, tissues were homogenized in RIPA buffer containing protease inhibitors (1 mM NaF; Sigma, #S-1504), 50 µg/ml aprotinin (Sigma, #A-6279), 1 mM sodium orthovanadate (Sigma, #S-6508), 1 mg/mL PMSF, and 10 mM PBS. Protein samples were diluted in 4X Laemmli sample buffer (Bio-Rad, #1610747) with 50 mM DTT and 10% β-mercoptoethanol, and solubilized at room temperature for 30 min. Ten µg of protein were resolved per lane on 4-12% Mini PROTEAN® TGX Stain-Free™ precast gels (Bio-Rad, #4568086 or #4568083) and transferred to Immun-blot® Low-Fluorescence PVDF membranes (Millipore, MA # IPVH00010) at 100V for 50 minutes as per manufacturer's instructions. Membranes were blocked in 5% (w/v) skim milk powder (Nestle Carnation, USA), PBS with 0.1% Tween-20 (PBST; blocking buffer) for 1 h, and incubated in rabbit anti-DMD (1:250; Abcam 15277) diluted in the same buffer overnight at 4°C. Membranes were rinsed twice in 0.1% PBST, and twice in blocking buffer for 10 min prior to a 1 h incubation in horseradish peroxidase (HRP)-conjugated

anti-rabbit IgG secondary antibody (1:2000; Jackson ImmunoResearch, #711-035-152) diluted in blocking buffer. Chemiluminescent signal was detected using the ChemiDoc™ MP imaging system (Bio-Rad #1708280).

2.7 Behavioural Phenotyping

2.7.0 Test Schedule

Experimental mice (*n* = 11 WT, *n* = 12 *mdx*) underwent a battery of behavioural tests starting at 10 weeks +/- 2 weeks of age. The order of testing is depicted in figure 7. Briefly, mice were consecutively subjected to the following tests: nest building (NB), light-dark box (LDB), marble burying (MB) and open field (OF). After a 1-week break, mice were subjected to the MWM for 11 consecutive days, followed by fear conditioning (FC) 3-6 days later. For each test with the exception of FC, mice were habituated in the testing room for one hour prior to experimentation. All mice were subjected to the same battery of behavioural tests, and no mice were excluded from the study.

2.7.1 NB

Mouse cages were prepared with bedding and a single nestlet (5cm x 5cm; Ancare). Two pictures were taken of the nestlet in each mouse cage prior to experimentation – one from a bird's-eye view and the second from the side (figure 8A). Mice were singly placed in these cages at ZT 11 and removed at ZT 2 the following day. Upon mouse removal, two pictures were again taken of each nestlet from the same angles (figure 8B). NB was scored on a scale of 1 to 5 by three independent investigators, blinded to the mouse genotype, using a standardized scoring sheet

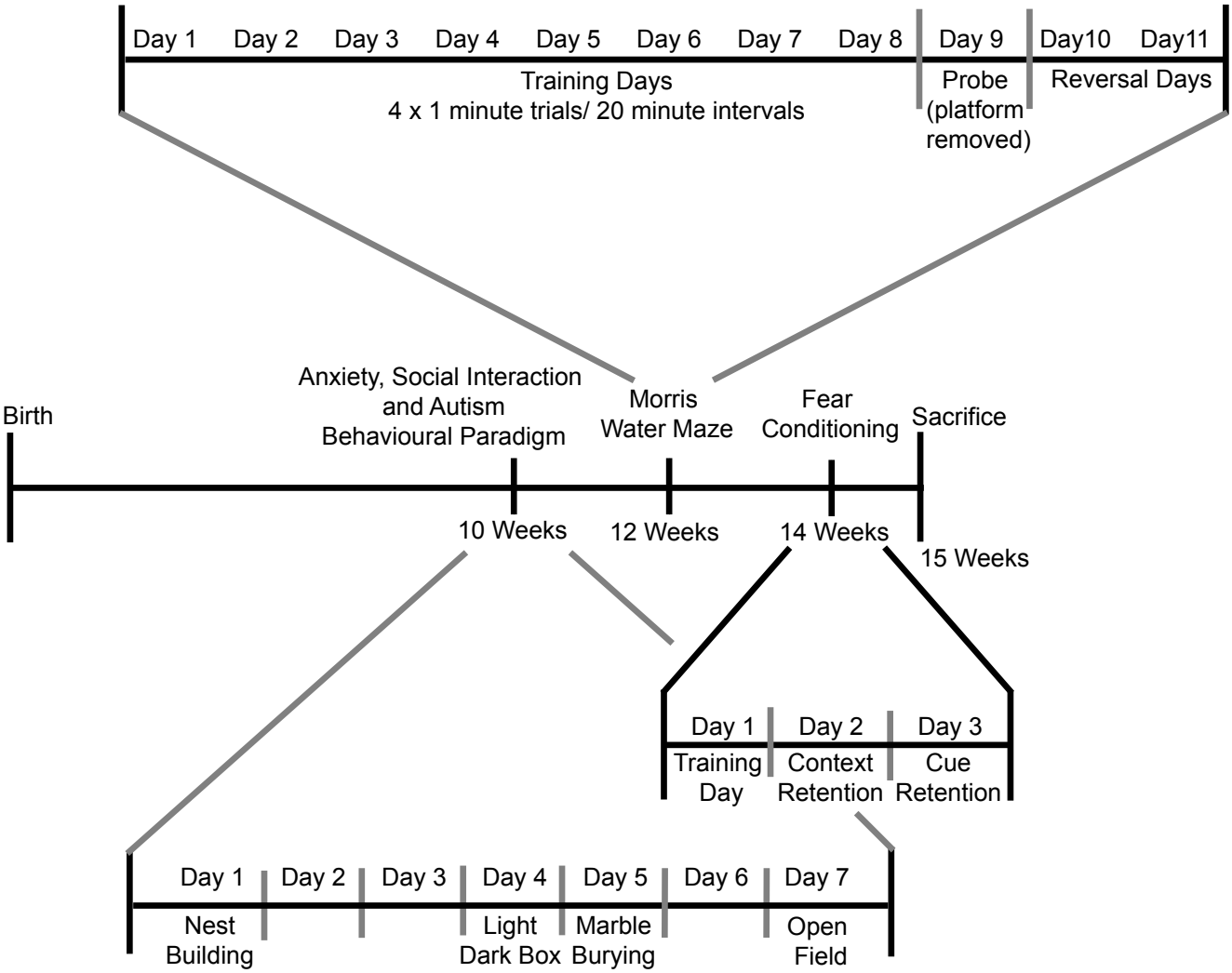

Figure 7 Timeline for behavioural testing. Behavioural tests performed assessed anxiety, autism-related behaviours, learning and memory and spontaneous exploration in age-matched, male WT (*n*=11) and *mdx* (*n*=12) mice.

A. Before

B. After

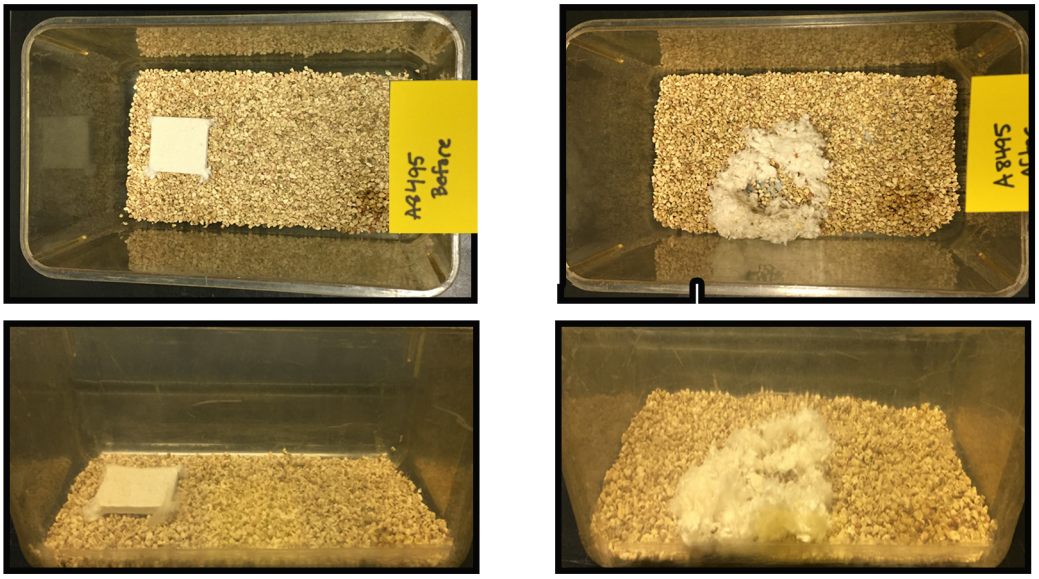

C.

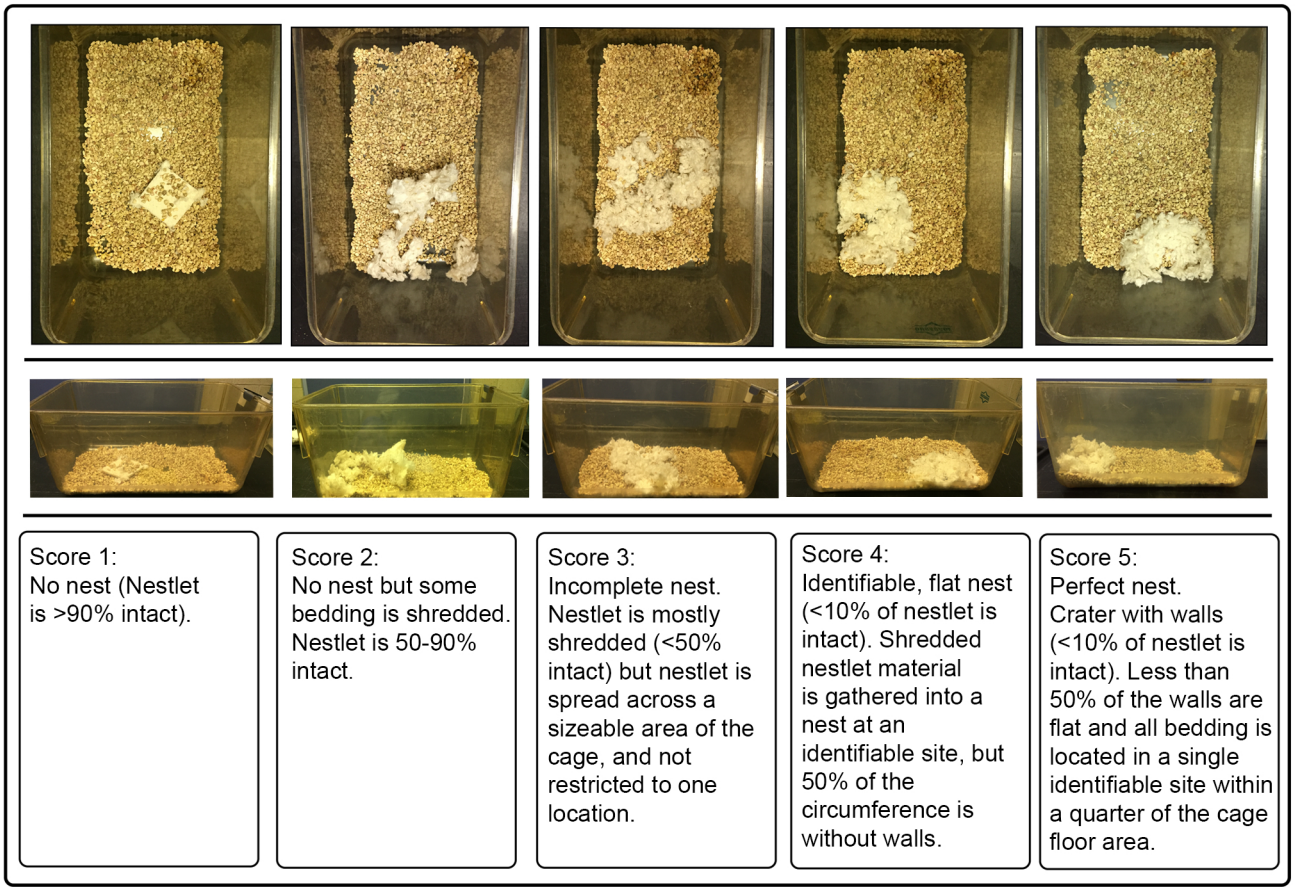

Figure 8 Scoring criteria used by investigators to assess repetitive behaviours in the NB paradigm. Pictures were taken from birds-eye-view and side of cage (A) before the mouse was placed in the cage (B) after the mouse was removed from the cage at the end of the test. (C) Scoring criteria used by three independent investigators. Nests were scored on an integer scale from 1-5. Adapted from Deacon *et al*, 2006.

developed by the Bennett lab, adapted from (Deacon, 2006), shown in figure 8C. Nest scores were plotted as the mean of the mode.

2.7.2 LDB

The LDB (Med Associates) consisted of a chamber with evenly sized dark and light compartments (28.7 cm x 15 cm x 20.6 m). The light side of the chamber was brightly lit (390 lux). Individual mice were placed in the light side of the chamber at ZT 3 and mouse activity was recorded for 10 minutes using a photobeam-based tracking system. The number of transitions and amount of time spent in each compartment was recorded.

2.7.3 MB

MB is a behavioural test to assess repetitive behaviours seen in autistic-like phenotypes. MB was conducted in a standard rat cage (26 cm X 48 cm x 20 cm) filled with 5 cm of SANI-chip bedding (Teklad, #7090). Twenty marbles (42 mm diameter, average weight 5.0 g, Miss Tiddlywinks) were evenly distributed on top of flattened SANI-chip bedding in 5 rows of 4, separated by 2 cm, measured using a cardboard cut-out created in-house). Two 'before' pictures were taken prior to the introduction of the mouse to the cage, one from a birds-eye view (figure 9A) and a second from the side view which included the experimental mouse ID (figure 9B). Mice were individually placed in cages at ZT 3 for a trial duration of 30 minutes. A picture was taken from a birds-eye view in a similar fashion as before the experimentation (figure 9C). Three independent investigators, blinded to mouse genotype, scored the number of marbles buried during the trials using criteria adapted from Deacon, 2006. Investigators counted the number of marbles visible from the birds-eye view photo, where a marble was scored as "buried" if at least 2/3 of its surface area were covered by bedding in the photo.

A. Before

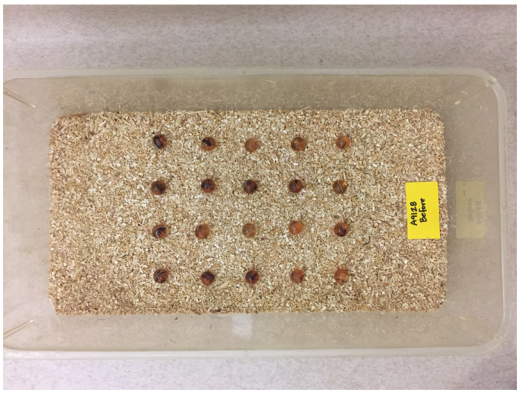

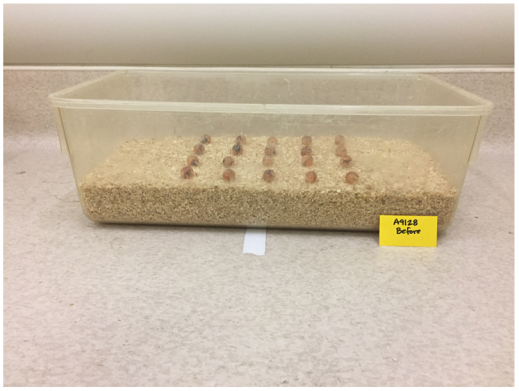

B. After

Figure 9 Representative photos of the MB paradigm. Pictures were taken (A) before and (B) after mice were placed in the MB cage.

2.7.4 OF

Mice were placed in a white polyvinylchloride (PVC) box (50 cm x 50 cm x 35 cm) illuminated by overhead light maintained at 300 lux. Mice were recorded by an overhead camera and tracked using Ethovision XT11.5 software. The boxes were cleaned with 70% ethanol between animals. The amount of time mice spent in the center and the periphery of the chamber was recorded. Trials started at ZT 3 and lasted 10 minutes.

2.7.5 MWM

The MWM was used to assess spatial learning and memory. The apparatus consisted of a plastic pool measuring 132 cm in diameter, filled with water that was kept at a constant temperature of 22°C and made opaque with non-toxic paint (506-BT12801O, Scholar's Choice). The pool was divided into four equally sized quadrants and a 10 cm diameter circular escape platform was placed 1 cm below the water surface, 24 cm away from the pools edge in the back-right quadrant. Two visual cues were placed on the walls of the room – a black "X" on the wall nearest the front quadrant of the pool and a black square on the wall nearest the left quadrant of the pool. Overhead lighting was maintained at 100 lux, and a white noise generator (2325-0144, San Diego Instruments) maintained background noise at 70 dB. Mice underwent eight testing days consisting of four trials separated by 20-minute inter-trial intervals. Each trial began when the mouse was placed randomly in one of the four equidistant locations of the pools edge and concluded when either the mouse independently found the platform, or the timer reached 60 seconds. Mice that did not find the platform on their own were guided to the platform by the experimenter where they remained for 20 seconds before being removed from the pool. On day nine, known as probe trial, mice underwent a single trial where the platform was removed, and mice were placed in the pool

in randomized quadrants for 60 seconds to test for reference memory. On the final two days of testing, known as reversal days, the platform was placed in the front left quadrant (opposite from the eight training days) and escape latency measured, similar to the training days. For all trials throughout MWM, mice were recorded using an overhead camera (Bosch, LTC0355/20; Pentax 3.5 – 8 mm Ins, TS2V314BED) and tracked using Ethovision XT11.5 (Noldus) Information Technology). Variables measured include: escape latency, average velocity, distance travelled on training and reversal days, and time spent in platform zone on probe. Mice began testing at ZT 8 for all eleven days.

The search strategies the mice employed in the MWM was assessed using software developed by the Bennett laboratory using criteria adapted from Janus (2004) and Brody and Holtzman (2006). This software assessed the swim pattern of each trial from the first eight days to infer the search strategy each mouse used. There are three search strategies: (i) looping (ii) systematic and (iii) spatial. Looping is a repetitive circling approach where mice swim either in small, tight circles or wider, concentric circles. Systematic strategies were defined as a non-spatial navigational approach where the mouse shows no preference for the target quadrant and includes randomly searching the inside of the tank without spatial bias. Spatial strategy represents an approach where the mouse swims directly to the platform or shows bias for the target quadrant over the entire trial. Floating was a behaviour that was also assessed to identify mice that lack intentional search strategy. A floating phenotype was defined as a mouse that has an average velocity under 6 cm/s and an escape latency of over 50 seconds a given trial. Mice that met floating requirements for more than four of the eight test days were excluded from the study. No mice were excluded from this study.

2.7.6 FC

Associative learning was assessed using fear conditioning (FC), a three-day paradigm consisting of a training (day one), context retention (day two) and cue retention (day three) trial each lasting 6 minutes. The apparatus used were PhenoTyper boxes (30 cm x 30 cm x 35 cm) illuminated by white light (100 lux) over a metal grid floor. On day 1 (training) mice received two tone-shock pairings (conditioned stimulus was a 30 second tone, and unconditioned stimulus was a 2 second foot shock). The first tone-shock pairing was administered at 2 minutes, and the second tone-shock pairing occurred at 3.5 minutes. On day 2 (context retention) mice were re-introduced to the same chamber as the previous day, in the absence of either tone or shock. On the third day (cue day) the apparatus was modified ensuring the previously known environment was unrecognizable. Cardboard inserts were used to change the shape of the chamber from square to triangular, weigh boats (Sigma, #W2751) filled with artificial vanilla (Clubhouse, #066200013257) were placed behind these inserts to adjust the odor, and ACVS cleaning solution was used between trials. Red lights and white noise (65 dB) replaced the previously white light and soundless chambers. A (80 dB) tone played for the final 3 minutes of the 6-minute test without an accompanying shock. Mouse freezing behaviour over the trials was collected using Ethovision XT11.5 software. For all days testing began at ZT 8 with no habituation.

2.7.7 Statistics

Data were analyzed using GraphPad Prism 7.0 software, where $p < 0.05$ were considered significant. Data were presented as the mean ± standard error of the mean (SEM). Groups of two were analyzed using an unpaired Student's *t* test, and groups of three or more were analyzed using a two-way ANOVA followed by Holm-Sidak *post hoc* analysis as indicated in all figure captions.

A repeated measures two-way ANOVA was used for escape latency and distance travelled during 8 training days in MWM.

3 RESULTS

3.1 Loss of Dp427 alters ANSC symmetric and asymmetric cell division

3.1.1 The *mdx* mice have fewer viable ANSCs compared to WT

A schematic of the protocol is presented in (figure 10A). WT mice had both more primary and secondary NSPs per well than *mdx* mice (figure 10B). WT mice also had a greater number of viable cells per well in primary and secondary NSP culture compared to *mdx* mice (figure 10C).

3.1.2 The *mdx* mice have larger secondary NSPs than WT

WT mice had larger primary NSPs than *mdx* mice (figure 10D-F). The *mdx* mice had larger secondary NSPs than WT (figure 10G-I). The distribution of NSP sizes are depicted in Figure 10J. The majority of mdx primary NSPs had an area less than 11,000 μm^2 whereas WT primary NSPs had greater variance in area (figure 10K).

3.2 Loss of Dp427 in *mdx* mice does not cause cognitive impairments.

3.2.1 The *mdx* mice do not show heightened levels of anxiety

Given the dramatic changes in NSP phenotype, we investigated the *mdx* mice for behavioral and cognitive alterations. To determine whether *mdx* mice were more anxious than WT controls, LDB and OF were performed. In LDB, the amount of time spent in the light compartment and the number of transitions to the light compartment were measured. There was no difference in the amount of time WT and *mdx* mice spent in the light zone ($p = 0.7031$; 11A), or

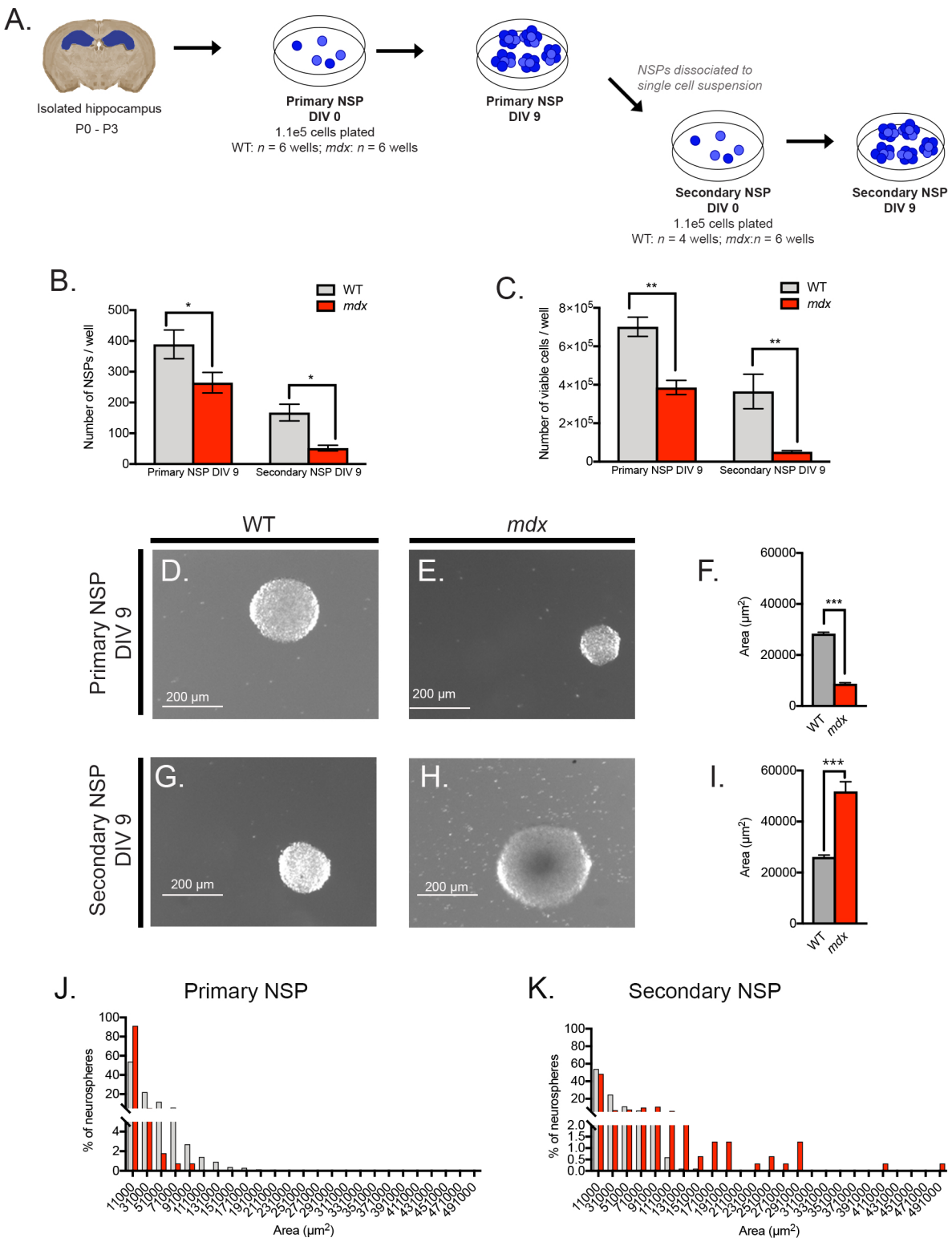

Figure 10 Dp427 has a role in type 1 and type 2 ANSC division in the SGZ of hippocampus. (A) Schematic of NSP assay. (B) WT mice generate more primary NSPs (*$p < 0.05$) and secondary NSPs (*$p < 0.05$) than *mdx* mice. (C) Cell number per well is greater in WT compared to *mdx* cultures, following primary NSP dissociation (**$p < 0.01$) and secondary NSP dissociation (**$p < 0.01$). In (B-C) statistics were two-way ANOVA, followed by *post hoc* Holm-Sidak. Representative images of (D) WT (E) *mdx* primary NSPs. (F) WT NSPs are significantly larger than *mdx* (unpaired Student's *t*-test, ***$p < 0.001$). Representative images of (G) WT and (H) *mdx* secondary NSPs. (I) *mdx* NSPs are significantly larger than WT (unpaired Student's *t*-test, ***$p < 0.001$). (J) Distribution of primary NSP size in WT and mdx cultures. Note the higher proportion of smaller primary NSP in *mdx* cultures (K) Gradual distribution of secondary NSP in WT and increased proportion of larger secondary NSP in *mdx* mice. Data represent: $n = 3$ WT and $n = 3$ *mdx* mice.

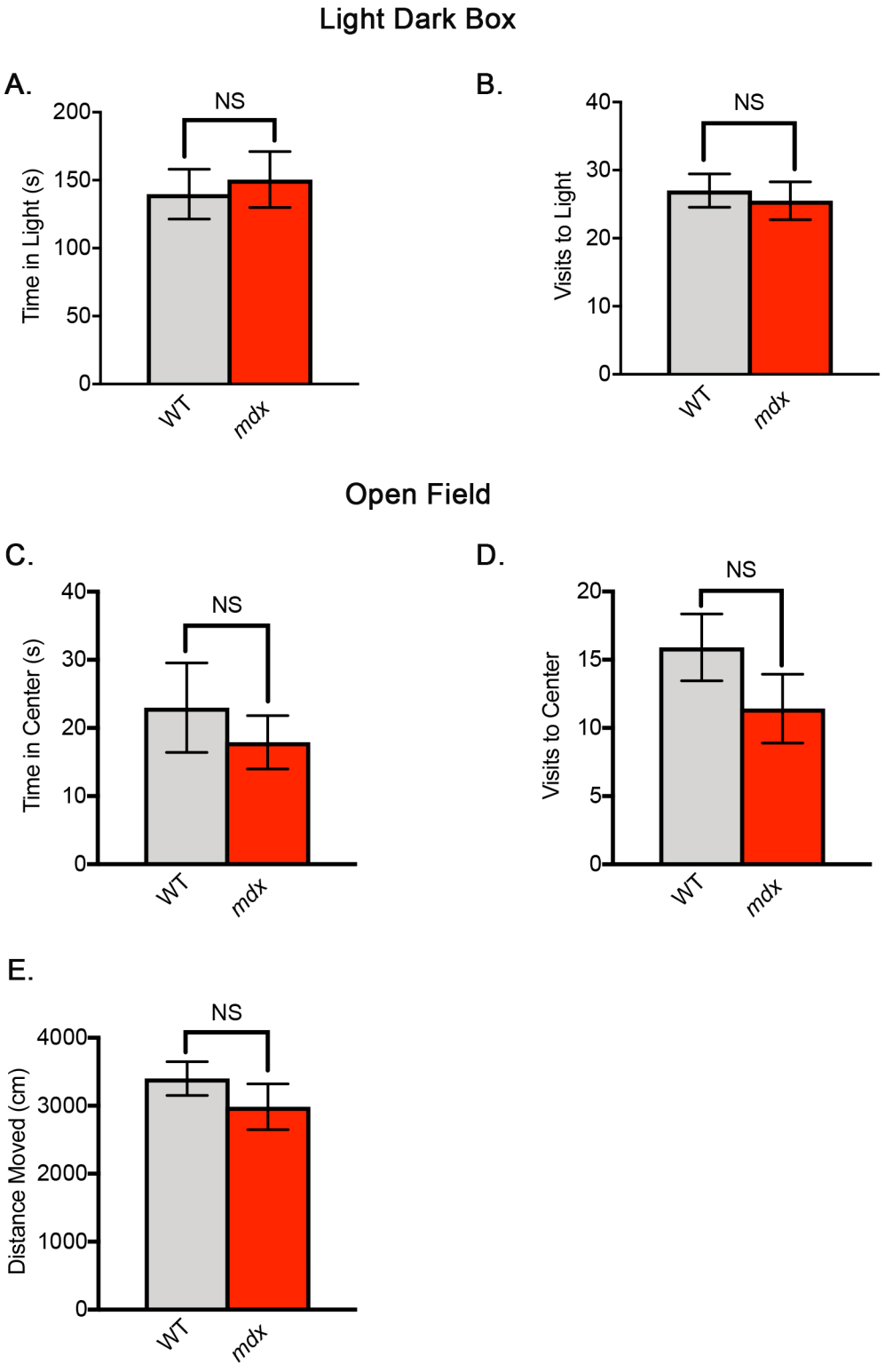

Figure 11 The *mdx mice* show normal levels of anxiety. In LDB, there was no difference between *mdx* and WT mice in (A) the amount of time spent in light compartment [$t = 0.3864$, df = 21, $p > 0.05$], or in (B) the number of visits to the light compartment between WT and *mdx* [$t = 0.4014$, df = 21, $p > 0.05$]. In OF there was no difference in (C) time spent in center of OF [$t = 0.6764$, df = 21, $p > 0.05$], (D) number of visits to the center of chamber [$t = 1.273$, df = 21, $p > 0.05$] or the (E) total distance moved in OF [$t = 0.9817$ df = 21, $p > 0.05$]. In A - E, statistics were unpaired Student's *t*-test, where $p < 0.05$ was considered signficant. Data represent $n = 11$ WT and $n = 12$ *mdx*.

number of transitions (p = 0.6922; figure 11B). In OF, the amount of time spent in the center of the field and the number of transitions to the center of the field were measured. There were no differences in time spent in center of OF (p = 0.5061; figure 11C) or in the number of transitions between the light and dark compartments (p = 0.2168; figure 11D). The total distance moved was also measured in OF to ensure there were no motoric impairments affecting the results of the test. As shown in figure 11 E, there was no difference between genotypes (p = 0.3374).

3.2.2 The *mdx* mice do not exhibit autistic-like behaviours

Stereotypy and perseverative behaviors were assessed using NB and MB. As shown in figure 12A, WT and *mdx* mice built similar quality of nests (p = 0.5499) and buried similar numbers of marbles (p = 0.1996; figure 12B).

3.2.3 The *mdx* mice do not exhibit learning and memory deficits

Learning and memory of the mdx mice was assessed using the MWM. For each mouse, escape latency was averaged across the 4 trials per day during the eight training days. A main effect of time was detected but there were no differences between *mdx* and WT escape latencies indicative of comparable learning curves (p = 0.3804; figure 13A). Motoric ability was also comparable between WT and *mdx* mice (figure 13B/C). Spatial learning and memory was assessed in a probe trial. Both WT and *mdx* spent more time in the correct quadrant than expected by chance. There were no differences between genotypes (p = 0.9466; figure 13D). On the final two days of testing, the platform was moved from the BR quadrant to the front left (FL) quadrant of the pool, and escape latency was measured. Both WT and mdx showed a reduced escape latency on day 11

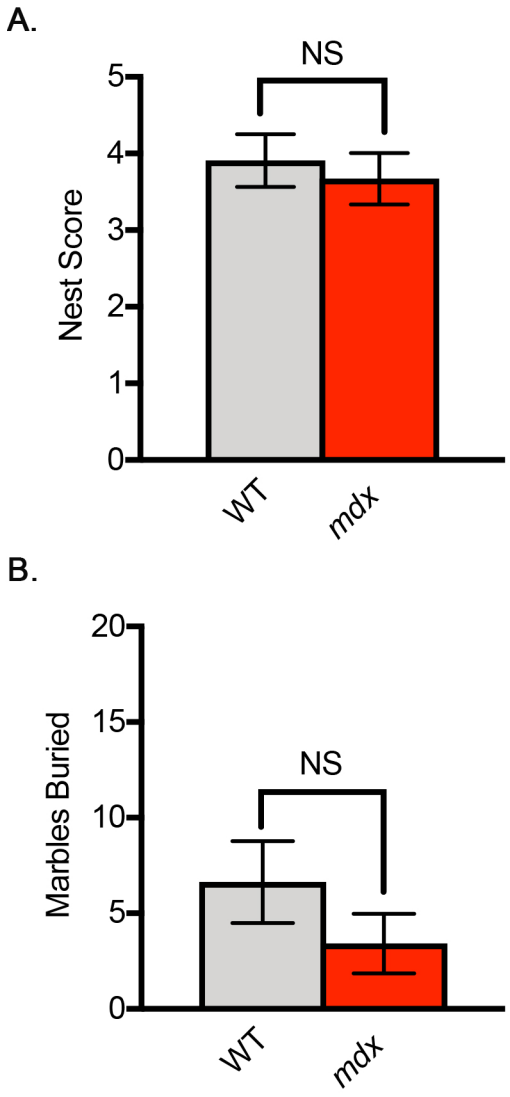

Figure 12 Loss of Dp427 does not elicit autism-related behaviours. (A) Nest quality was similar between WT and *mdx* mice, ranked on a score of 1-5 (Mann Whitney $U = 55$, $p > 0.05$) . (B) WT and *mdx* mice buried similar number of marbles (Mann Whitney $U = 46$, $p > 0.05$) . In A-B, statistics used were unpaired Mann-Whitney U test, where $p < 0.05$ was considered significant. Data represent $n = 11$ WT and $n = 12$ *mdx* mice.

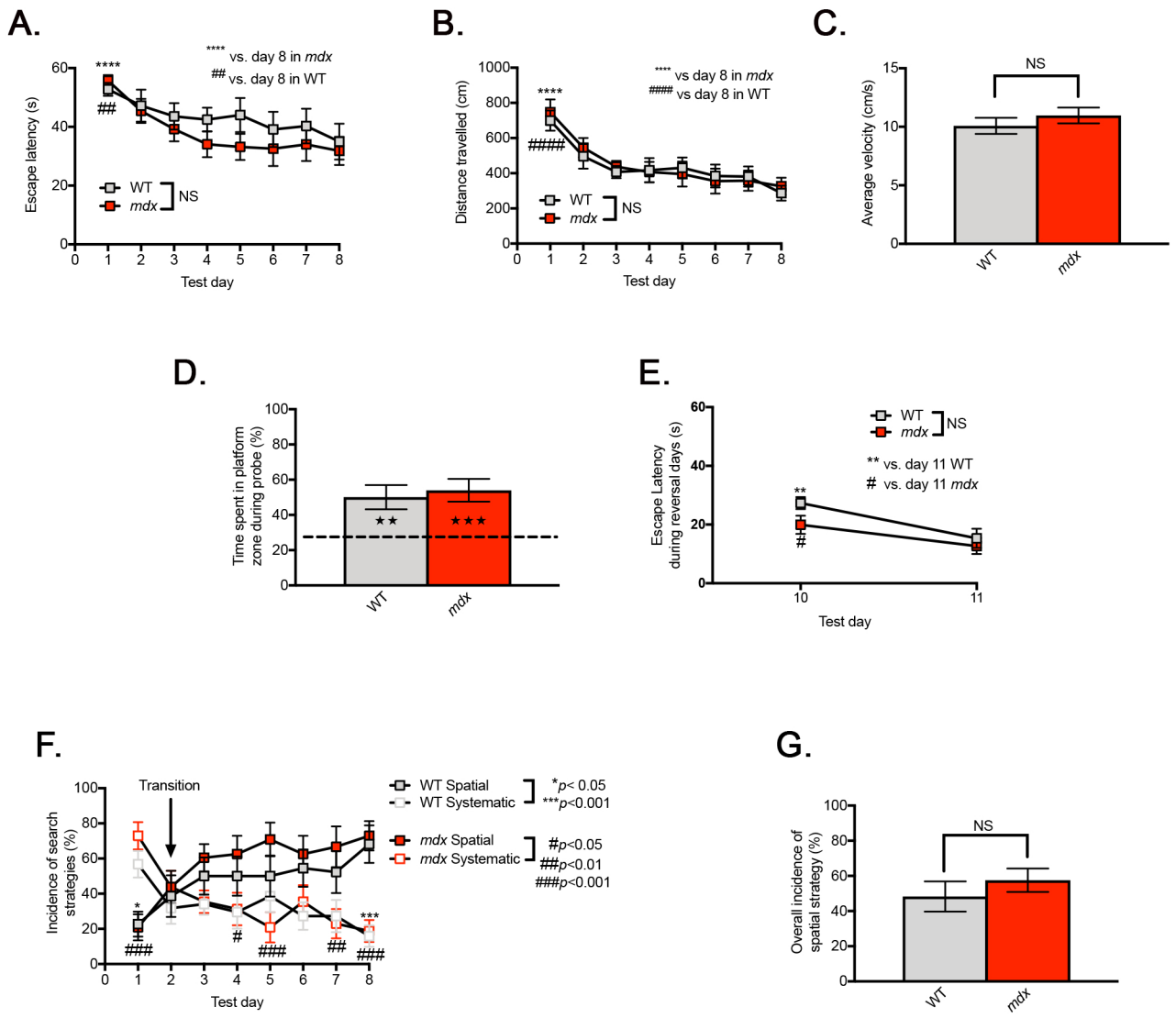

Figure 13 The *mdx* mice exhibit similar spatial learning and memory to WT. (A) Escape latency improved for both WT and *mdx* mice by day 8 (two-way repeated measures ANOVA: main effect of time, $F_{(7, 147)}$ = 8.518,WT: ###p < 0.001, *mdx*: ****p < 0.0001, *post hoc* Holm-Sidak multiple comparisons). There was no genotypic difference in escape latency ($F_{(1,21)}$ = 0.8028, p > 0.05, *post hoc* Holm-Sidak multiple comparisons). (B) Both WT and *mdx* mice showed reduction in distance swam over 8 training days (two-way repeated measures ANOVA: $F_{(7,147)}$ = 11.92, WT: ****p < 0.001, *mdx*: #### p < 0.001, *post hoc* Holm-Sidak multiple comparisons) but there was no main effect of genotype (two-way repeated measures ANOVA: main effect of genotype, $F_{(1,21)}$ = 0.03367, p > 0.05, *post hoc* Holm-Sidak multiple comparisons). (C) WT and *mdx* mice swam at comparable velocities (unpaired Student's *t*-test, t = 0.9214, df=21, p > 0.05). (D) Both WT and *mdx* mice showed a preference for the platform zone during the probe test (one-sample t-test: WT: t = 3.638, df = 10, ***p < 0.0001; *mdx*: t = 4.47, df = 11, **p < 0.001 compared to 25% (random chance, hashed line), but no genotypic difference (unpaired Student's *t*-test: t = 0.4123, df = 21, p > 0.05). (E) Escape latencies for both WT and *mdx* gradually declined during reversal days (two-way repeated measures ANOVA, main effect of time, $F_{(1,21)}$ = 17.19, WT: **p < 0.01, *mdx*: #p < 0.05 indicating main effect of time) yet there was no main effect of genotype (two-way repeated measures, ANOVA: $F_{(1,21)}$ = 2.355, p > 0.05). (F) On training day one, both WT and *mdx* mice used a systematic search strategy, then transitioned on day two to a spatial approach. There was no main effect of genotype (two-way repeated measures ANOVA: main effect of genotype, $F_{(1, 21)}$ = 0.7449, p > 0.05. #p < 0.05, ##p < 0.01, ###p < 0.01 vs spatial strategy) (G) Overall incidence of spatial search strategy did not differ between WT and *mdx* (unpaired Student's *t*-test, p > 0.05).Data represent n = 11 WT, and n = 12 *mdx* mice.

compared to day 10 ($p = 0.0005$) with no differences between genotypes ($p = 0.1398$; figure 13E).

We next evaluated the search strategies employed over the eight days of training. As shown in figure 13F, when initially placed into the MWM on day 1, both *mdx* and WT mice used a predominantly systematic approach to finding the platform (WT: $p = 0.0299$; *mdx*: $p = 0.0002$). Following the transition on day 2, WT mice employed a spatial search strategy for the remainder of the test days. Similar to WT, *mdx* mice adopted a spatial search strategy on day 2, as both genotypes transitioned from systematic to spatial search strategy. Starting on day four ($p = 0.04$), mdx mice used a predominantly search spatial strategy which they maintained for the remainder of test days 5 ($p = 0.0003$), 7 ($p = 0.002$) and 8 ($p = 0.0001$). The overall incidence of the spatial search strategy did not differ between WT and mdx mice during the 8 training days: 1 ($p = 0.9979$), 2 ($p = 0.9614$), 3 ($p = 0.77639$), 4 ($p = 0.6550$), 5 ($p = 0.2604$), 6 ($p = 0.8752$), 7 ($p = 0.5532$) and 8($p = 0.9689$; figure 13G).

3.2.4 Associative learning and memory is enhanced in *mdx* mice

FC was used to further assess learning and memory, which pairs a negative stimulus (foot shock) with a neutral stimulus (tone). Freezing behaviour is measured in each of the three testing days, where more time spent freezing is indicative of learning and memory. During the training day (figure 14A), both *mdx* and WT mice demonstrated significantly more freezing following the second tone-shock pairing relative to the first exposure (WT: $p = 0.0019$, *mdx*: $p = 0.0399$). There was no genotypic difference in freezing following the first tone-shock ($p = 0.4214$), or the second ($p = 0.1479$).

A. Training

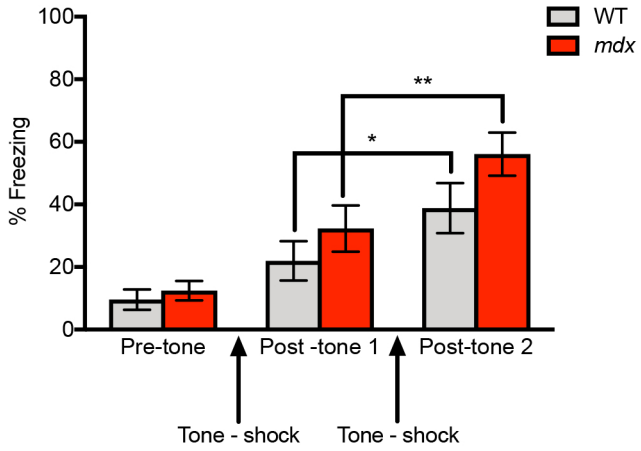

B. Context Retention

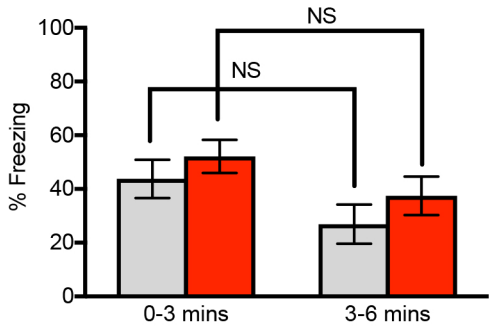

C. Cue Retention

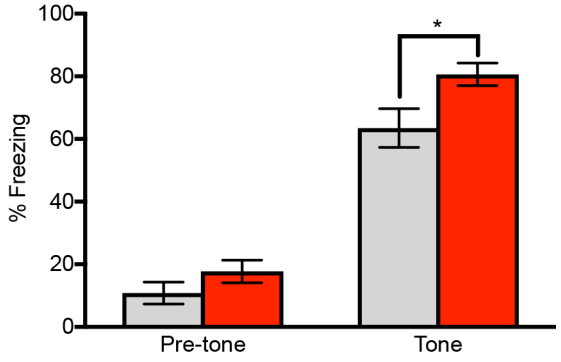

Figure 14 Associative learning was enhanced in *mdx* mice. (A) WT and *mdx* had a higher incidence of freezing following the second CS-US (tone-shock) pairing on training day (two-way ANOVA: main effect of time, $F_{(2,42)} = 28.48$, *$p<0.05$, **$p < 0.01$, *post hoc* Holm-Sidaks multiple comparisons), but there was no statistical difference between the genotypes ($F_{(1,21)} = 2.31$, $p > 0.05$). (B) The incidence of freezing was comparable between genotypes during context retention, the second day of testing (unpaired Student's *t*-test $t = 1.27$, df = 21, $p > 0.05$). (C) *mdx* mice froze more than WT mice following the CS (two-way ANOVA: main effect of genotype, $F_{(1,21)} = 6.199$, *$p < 0.05$, *post hoc* Holm-Sidaks multiple comparisons).

The absence of tone on the second test day (context retention) establishes if the mice are able to associate the environment with the negative stimulus. There was no statistical difference between the first three minutes and the final three minutes for either genotype (WT: $p = 0.0651$, *mdx*: $p = 0.0651$; figure 14B).

On the third test day, mice were placed in a new environment and the 30-second tone was played at three minutes. As shown in figure 14C, mdx mice froze more compared to WT in response to the tone ($p = 0.0153$), demonstrating greater memory retention.

3.3 Novel mouse models did not achieve brain specificity, nor did they deplete target tissues of dystrophin

3.3.1 Specificity of the nestin promoters employed

IFC was used to qualitatively assess the tissue-specificity of three different nestin promoter constructs, all of which use the Cre-lox system. Recombination was assessed in the tibialis anterior and brain. Muscle isolation and IFC analysis was performed by Dr. Caroline Brun. Recombination in the brain was assessed in the SGZ of the DG as part of this thesis research.

In NestinCre^{ERT2} (SB1) R26R YFP$^{+/+}$ muscle, there was no recombination in muscle in absence or presence of TAM, confirming that the NestinCre^{ERT2} (SB1) promoter construct does not contain muscle-specific enhancer elements. In the brain, recombination occurred in the SGZ of the DG could, however, be detected in absence of TAM but was increased following TAM administration (figure 15A).

The NestinCre^{ERT2} (5.1) R26R-mT/mG$^{+/+}$ showed no clear recombination in muscle in the absence of TAM but did show recombination in the presence of TAM. In the brain, extensive recombination occurred within the SGZ only following TAM administration (figure 15B). These

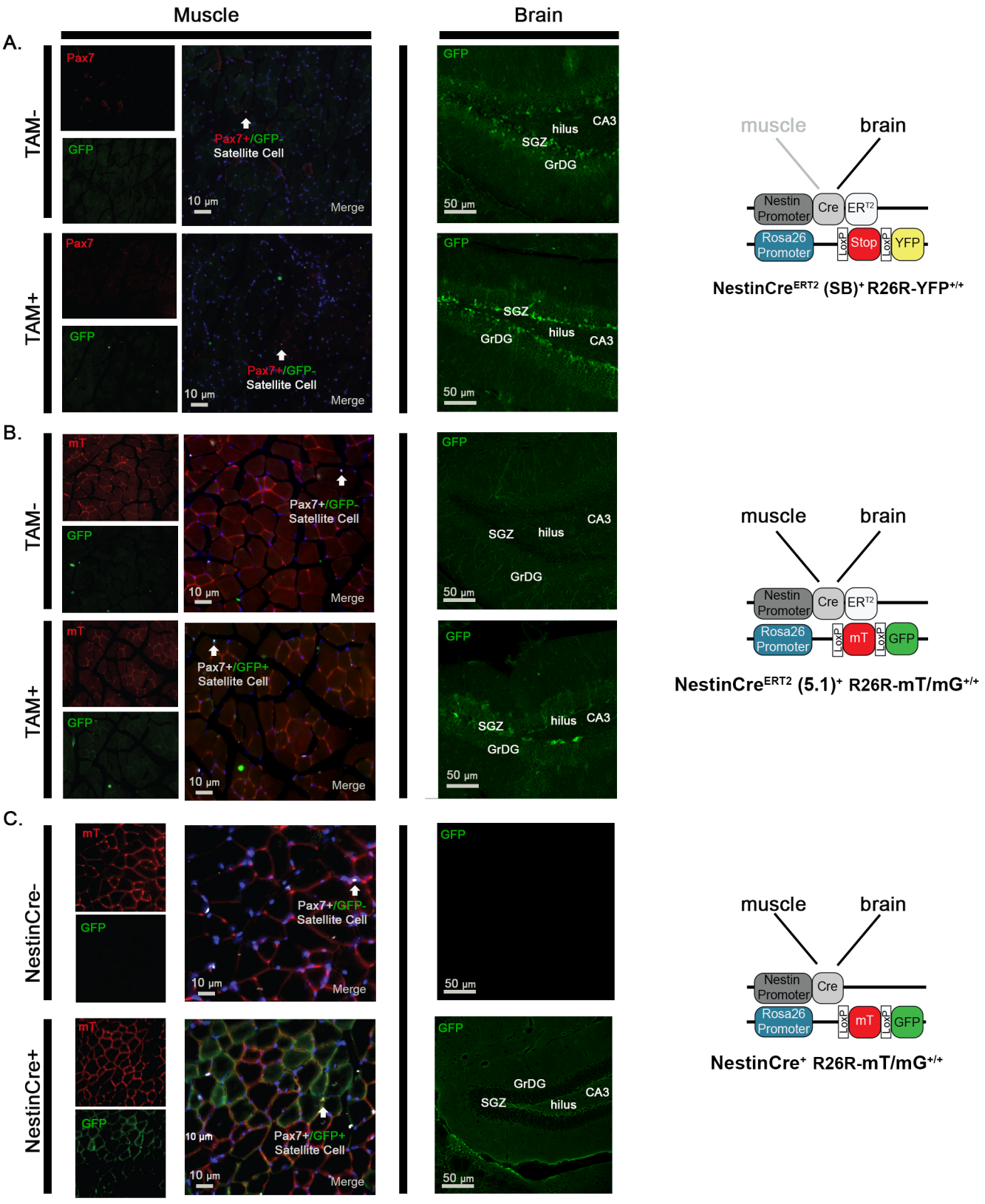

Figure 15 IFC reporter analysis of the three nestin-Cre and nestin CreERT2 promoter constructs in hippocampus and muscle. (A) The NestinCre^{ERT2} (SB) promoter construct is brain-specific, but exhibits some Cre-recombination in the absence of tamoxifen. (B) The NestinCre^{ERT2} (5.1) promoter does not show recombination in the absence of TAM, but contains both the muscle- and brain-specific enhancer elements. (C) The NestinCre promotor contains both the muscle- and brain-specific enhancer elements.

results demonstrate the NestinCreER$^{T2\text{-}5.1}$ promoter construct contains both the muscle and the brain specific enhancer elements and is inducible by TAM administration.

There was no recombination in the NestinCre^{-} mT/mG$^{+/-}$ muscle. There was recombination in the NestinCre^{+} mT/mG$^{+/+}$ muscle (figure 15C), indicating the presence of muscle specific enhancer elements in this promoter construct. Similarly, there was no recombination in the brain of the NestinCre^{-} mice. The NestinCre^{+} mT/mG$^{+/-}$ showed recombination demonstrating that this NestinCre promoter construct contained brain specific enhancer elements.

3.3.2 The constitutive fDMDH mouse line does not deplete any *DMD* isoforms in hippocampus or muscle

Using the Cre-lox system with the strongest recombination in brain (and muscle), we investigated whether Dp427 and its smaller isoforms were deleted in hippocampus and tibialis anterior muscle by western blotting. The NestinCre^{+} fDMDH$^{f/y}$ did not deplete any dystrophin isoform in hippocampus (figure 16A) nor muscle (figure 16B). The WT N15 mouse showed the presence of all dystrophin isoforms: Dp427, D140, Dp71 and Dp40 in hippocampus. These isoforms were present in muscle as well, with the exception of Dp40 which appeared to be completely absent in muscle from all mice tested. As expected, the *md*x mouse did not have Dp427 in both hippocampus and muscle. Interestingly, while all other dystrophin isoforms were present in *mdx* hippocampus, in muscle Dp140, Dp116, Dp71 and Dp40 were not present. There was no depletion of any dystrophin isoforms from our NestinCre^{+} fDMDH$^{f/y}$ tissue (muscle or brain, figure 16A,B) despite successful recombination of the reporter construct (figure 15C). Taken together, these data suggested that the loxP sites are too distal from each other to enable successful excision.

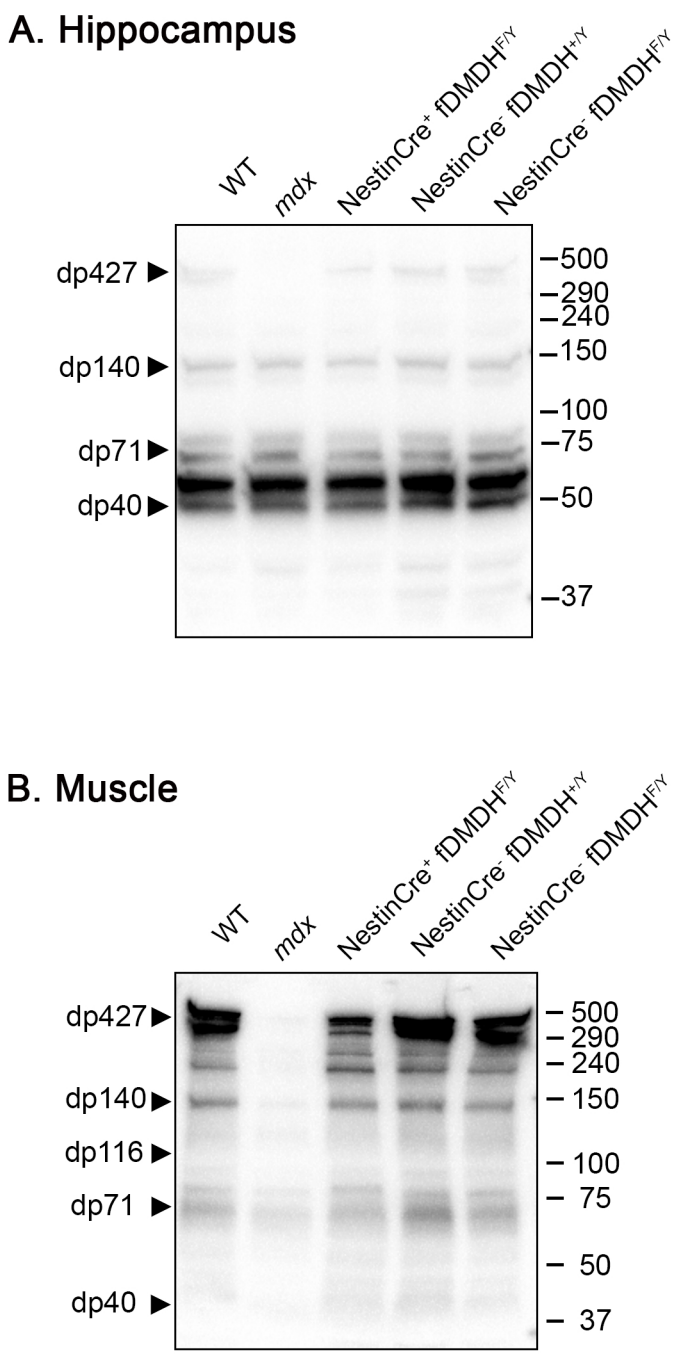

Figure 16 Dystrophin was not depleted from the hippocampus or muscle of the nestinCre fDMDHf/f mouse line. Immunoblots for dystrophin were performed using an antibody that recognizes all isoforms. Protein levels were comparable between WT N15, NestinCre^{+} fDMDH$^{f/Y}$, NestinCre^{-} fDMDH$^{+/Y}$, and NestinCre^{-} fDMDH$^{f/Y}$ mice. We used *mdx* mice as a postive control demonstrating that dp427 is depleted in this line. (Western blots were performed by Dr Stephanie Fowler in the Bennett laboratory).

4 DISCUSSION

In this thesis, my data suggest that Dp427 has a role in regulating symmetric and asymmetric division of ANSCs. Specifically, I found *in vitro* that the *mdx* mouse has fewer type 1 ANSCs and type 2a transit amplifying progeny and that have a greater propensity to divide symmetrically as assessed by comparing primary and secondary neurosphere size. Proposed mechanisms are described below. Despite this deficit, I show *in vivo* that loss of Dp427 in *mdx* mice has no effect on behavioural indices of anxiety or ASD-like phenotypes. Interestingly, my data demonstrate that while spatial memory is unaffected by loss of Dp427, associative fear learning is enhanced. To determine whether these phenotypes were modulated by the loss of additional dystrophin isoforms (Dp260, Dp140, Dp116, Dp71 and Dp40) from brain, I sought to generate brain-specific constitutive and conditional *DMD* knockout mouse models using three different NestinCre or NestinCre^{ERT2} promoter constructs. Although the floxed DMD allele employed in this study was not deleted in any of the models generated, I demonstrated that the NestinCre or NestinCre^{ERT2} promoter of two commonly used constructs contain both muscle- and brain-specific enhancer elements, while a third NestinCre^{ERT2} promoter construct contained only the brain-specific enhancer elements.

4.1 Loss of Dp427 disrupts ANSC division

The phenotype of ANSCs and type 2 transit amplifying neural progenitor cells described in this thesis, suggests that the balance between self-renewal and commitment is altered in ANSCs devoid of Dp427. I found that primary NSPs were fewer and smaller but that secondary NSPs were fewer *but larger* in in *mdx* compared to WT mice. This is the first characterization of ANSCs *in vitro* cultured from the SGZ of *mdx* mouse. My data are consistent with a single report

characterizing NSP phenotype cultured from the SVZ of *mdx* mice wherein mice have a reduced number of primary NSPs (Annese et al., 2016). Taken together, my data and that of Annese *et al*, 2016 suggest that loss of Dp427 reduces the number of ANSCs in the SGZ and has a role in their cellular division. When placed in context with studies of satellite cells cultured from *mdx* mice (Dumont et al., 2015), the ANSC phenotype described in this thesis is consistent with enhanced symmetric self-renewal division to slowly dividing ANSC *in vivo* ultimately leading to ANSC exhaustion indicative by fewer and smaller NSP cultures. Moreover, I show that when induced *in vitro* to generate secondary NSPs, consistent with Dumont et al., 2015, these secondary ANSC cultures switch fate, symmetrically specifying to two type 2a transit amplifying daughter cells generating fewer but larger NSPs than WT. The stem cell population size depends on the balance between self-renewal and cell differentiation (Ito and Suda, 2014). Under normal conditions, the majority of activated type 1 ANSC divide asymmetrically (Kronenberg et al., 2003; Bond et al., 2015), resulting in an equal number of type 1 ANSC daughter cells (self-renewal) that maintain the stem cell pool, and type 2a NPCs capable of specification (neurogenesis). In symmetric cell division, an activated type 1 ANSC will yield either two type 1 ANSCs or two type 2a NPCs (Bond et al., 2015). These two paths are shown in figure 17 comparing the WT phenotype to the *mdx* phenotype.

Primary NSP cultures reflect the number and intrinsic phenotype of ANSC cultures. By DIV9, the predominant cell types in primary NSPs are type 1 ANSCs and type 2a transit amplifying neural progenitor cells (Kronenberg et al., 2003). Both of these cell types are similar in size (Kempermann et al., 2004) but differ in rates of cellular division; type 1 ANSC are the slowest to divide and type 2a (also known as a transient amplifying cells) have the fastest rate of

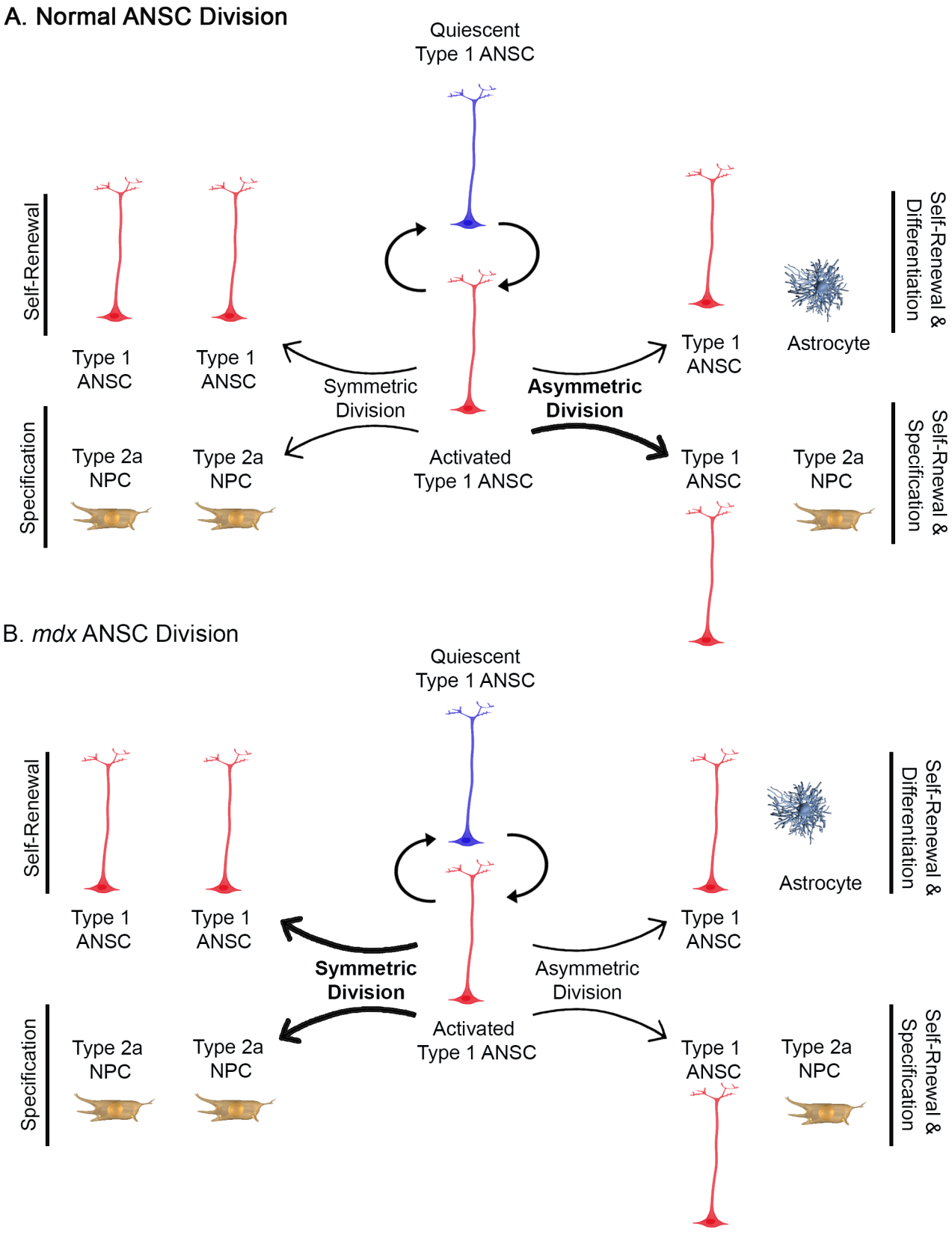

Figure 17 Proposed schematic of ANSC symmetric and asymmetric division in WT and *mdx* mice. (A) In WT ANSC division, most divisions are asymmetric producing a type 1 ANSC (self-renewal) and a type 2a NPC (specification). (B) In *mdx* ANSC division, the majority of divisions are symmetric, producing two type 1 ANSC (self-renewal) in primary NSP cultures, then switching to producing type 2a NPCs in secondary NSP cultures. Model adapted from that of WT division proposed in Petit *et al*, 2012; Bond *et al*, 2015.

division (Kronenberg et al., 2003). The data presented in this thesis suggests that the smaller primary *mdx* NSPs reflect an increased rate of symmetrical division producing two type 1 ANSCs. Interestingly, secondary *mdx* NSPs are fewer, but larger, than WT. This suggests that secondary *mdx* NSPs maintain preferentiality for symmetric division but shift from the production of two type 1 ANSCs to two type 2a neural progenitor cells. It remains unknown what signals ANSCs to divide asymmetrically versus symmetrically (Bond et al., 2015), but this thesis implicates dystrophin's involvement. In satellite cells, Dp427 is polarized to one side of the cell, which separates cellular components that are essential for determining cell fate and allows the cell to divide asymmetrically (Dumont et al., 2015). In the absence of Dp427, this polarity is lost, and the cell divides symmetrically (Dumont et al., 2015). My data are consistent with this mechanism in satellite cells supporting the claim that Dp427 has a critical role in establishing cell polarity and regulating division not only in muscle but also the hippocampus.

Integration of newly-born hippocampal neurons into pre-established networks is integral in learning and memory function, and is achieved through regulated, sequential cell division, differentiation, and specification (Mateus-Pinheiro et al., 2011). In the SGZ, activated type 1 ANSC, identified by nestin and glial fibrillary acidic protein (GFAP), can generate type 2a NPC (Swayne and Bennett, 2016). Both type 1 ANSC and type 2a NPC are multipotent, thus capable of self-renewal. A cell is committed to neurogenesis once a type 2a specifies to a 2b, which ultimately specifies to a type 3 DCX+ neuroblast. Figure 18 shows this specification process. Neuroblasts will ultimately migrate tangentially into the granule cell layer of the DG, where they differentiate into post-mitotic neurons (Swayne and Bennett, 2016). The NSP data shown here indicate that in the absence of Dp427, ANSC acutely proliferate, leading to stem cell exhaustion. This exhaustion will chronically reduce the number of proliferative cells capable of generating

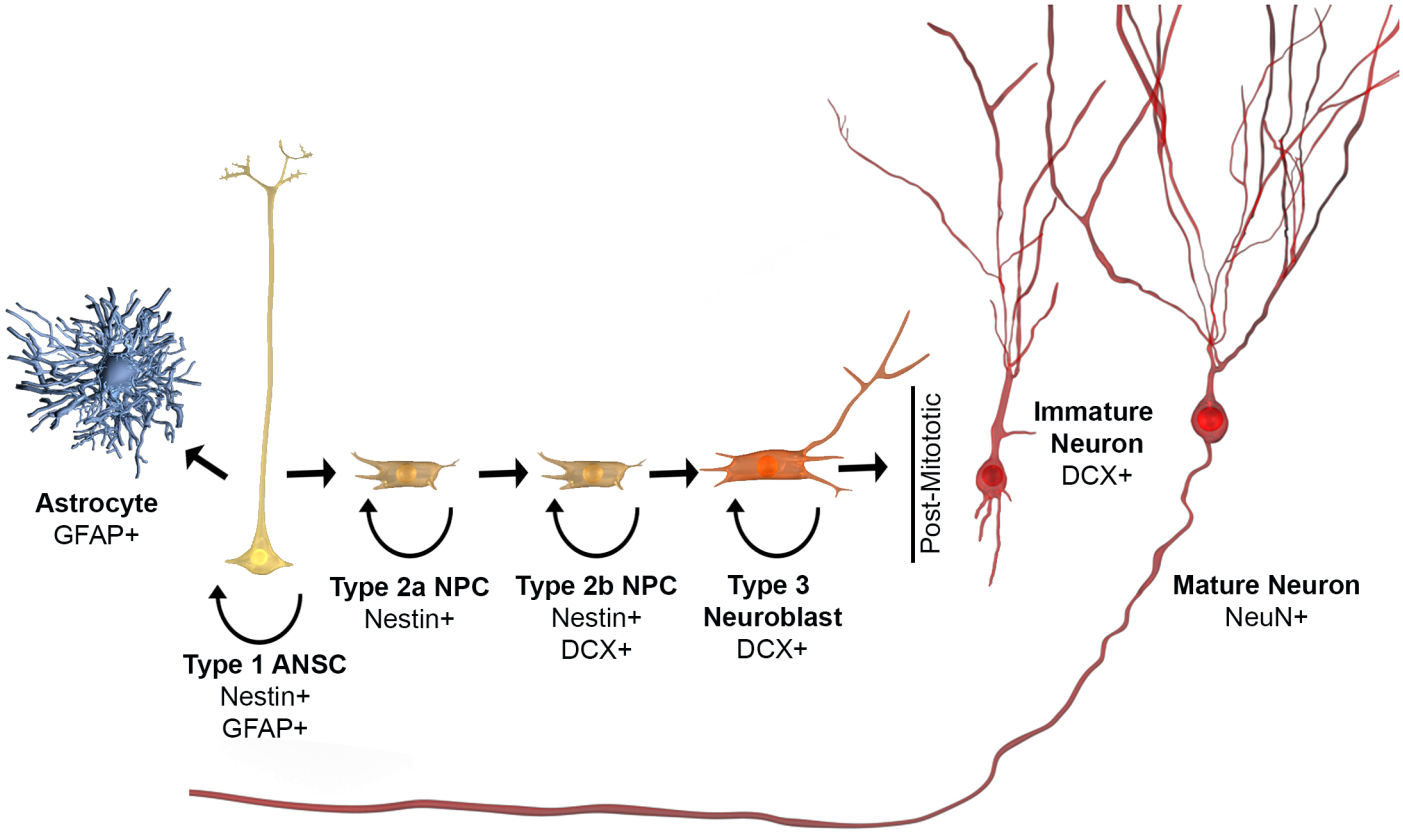

Figure 18 Schematic diagram of the specification process in the SGZ of the DG, and the antigenic markers used to follow this process. Adapted from Petit *et al*, 2012

new mature neurons and may have implications for the cognitive phenotype in DMD patients.

4.2 Cognitive profile of *mdx* mice

In this thesis I attempted to reconcile behavioural inconsistencies in the literature using the *mdx* mouse model. I show that male *mdx* mice do not have an anxious phenotype, do not exhibit repetitive ASD-like behaviors, and have normal spatial learning and memory. Interestingly, *mdx* mice were found to have enhanced fear associative memory with greater contextual retention memory than WT mice.

Sex differences is a major factor to consider when reconciling previous literature and assessing the biological relevance of a mouse model. Two previous studies determined female *mdx* mice were impaired in the LDB relative to WT (Remmelink et al., 2016), whereas male *mdx* were unimpaired (Vaillend et al., 1995). The first behavioural test on *mdx* mice to assess spatial memory concluded that male *mdx* were impaired in the T-maze (Vaillend et al., 1995), yet this finding was not echoed in female mice (Vaillend et al., 1995; Remmelink et al., 2016). It is important to note that (Remmelink et al., 2016) used female mice homozygous with the *DMD* mutation and (Vaillend et al., 1995) used male mice, suggesting the *mdx* mouse model may be sexually dimorphic. My data support Vaillend *et al*, 1995 indicating that that male *mdx* mice do not display an anxious phenotype in LDB.

While cognitive impairments are non-progressive in DMD patients, anxiety-associated behaviours appear to be developmental. DMD patients are most affected by anxiety at 12 years (Blake, 2002). This phenotype is not modelled in *mdx* mice. Tests using prepubescent *mdx* mice showed no difference in levels of anxiety in 6-week-old mice (Manning et al., 2014). Similarly, tests using older mice, 11 and 16 weeks, pubescent male mice showed no anxious phenotype (Vaillend et al., 1995; Sekiguchi et al., 2009; Manning et al., 2014). I clearly show here, consistent

with previous literature (Manning et al., 2014; Remmelink et al., 2016), that 10-12-week-old *mdx* mice showed no behavioural indices of anxiety in either the LDB or the OF compared to WT mice. It is possible that extrinsic factors may be responsible for this sudden peak of anxiety in DMD patients, or that *mdx* mice require a more stressful test to recapitulate the phenotypes seen in humans.

Prior to this thesis, ASD-like behaviour had been previously assessed in the *mdx* mouse model in a single study using tests measuring communication (i.e., ultrasonic vocalizations) and social interaction (i.e., male-female social interaction, male exposure to female urine and bedding, resident-intruder test and 3 chamber sociability; (Miranda et al., 2015). The authors suggested Dp427 may contribute to an autistic phenotype. However, stereotypies and perseverative behaviours were not tested in this study. A meta-analysis identified repetitive behaviors as part of the DMD syndrome (Snow et al., 2013). I directly addressed this issue here by investigating two assessments of ASD-like behaviours: nest building and marble burying associated with hippocampal dysfunction (Deacon et al., 2007). I found no evidence of DMD associated stereotypy or perseveration. The *mdx* mice built normal nests compared to WT. Similarly, a comparable number of marbles were buried between WT and *mdx*. Additionally, the reversal test in the MWM can be used to measure perseverance in mice (Silverman et al., 2010). Mice that fail to perform on reversal days could be seen as lacking the flexibility to switch from one location to another (Silverman et al., 2010), however *mdx* mice did not differ from WT. Taken together, these data indicate that *mdx* mice do not exhibit repetitive behaviours associated with ASD or DMD.

I found no evidence of non-progressive spatial learning impairment in *mdx* mice. Whether *mdx* mice have learning and memory impairments is ambiguous with conflicting reports in the literature. Consistent studies indicating learning and memory is not impaired in the *mdx* mouse

model (Sesay et al., 1996; Vaillend et al., 2004; Chaussenot et al., 2015) I found that spatial memory was unaffected by loss of Dp427 in the MWM. I further assessed whether WT and *mdx* mice could differ in cognition via the strategy they use to find the platform. There is a single report suggesting that *mdx* mice take a less direct path to the platform than WT mice (Chaussenot et al., 2015). In this thesis, I assessed a more granular metric of navigational strategy concluding that WT and *mdx* are indistinguishable in their capacity to adopt increasing effective MWM search strategies over time. I show here that both *mdx* and WT mice transition from a primarily systematic to a primarily spatial search strategy at the same rate. Thus, unlike previous literature (Chaussenot et al., 2015) I conclude that both learning process and learning success does not differ between *mdx* and WT mice.

While spatial memory remains intact in *mdx* mice, it is not known if associative memory is affected by loss of Dp427. Previous findings suggested that *mdx* mice had both associative, long-term, and cue-retention memory impairments (Muntoni et al., 1991; Chaussenot et al., 2015) while contextual memory retention was unaffected (Chaussenot et al., 2015) . I show in this thesis that both genotypes demonstrate equal associative memory in capacity for tone-shock pairing, however, not only do *mdx* mice have enhanced functional cue retention memory, as they have higher incidence of freezing behavior following introduction of the tone. These results are not a result of increased sensitivity of the *mdx* mouse, as both genotypes have similar foot shock response profiles (Chaussenot et al., 2015). Improved associative memory in *mdx* mice provides information on the role of Dp427 in regulating emotional components of memory in DMD patients.

While there are individual cognitive and behavioural profiles (Mehler, 2000) an overall cognitive profile in DMD patients exists regardless of the severity of non-progressive intellectual impairment (Hinton et al., 2000; Chaussenot et al., 2015). Common impairments in DMD patients

include: short-term memory, verbal comprehension, and limited verbal/auditory span (Hinton et al., 2000). In this thesis, I show that male *mdx* mice do not have an anxious phenotype, do not exhibit repetitive behaviors typical in ASD, and have normal spatial learning and memory. However, *mdx* mice have enhanced associative memory, with greater cue retention memory than WT mice. Information regarding the tone and shock in FC is transmitted to the amygdala, a structure important for associative learning and memory (LeDoux, 2000). Dystrophin is found in the basolateral amygdala (BLA) of healthy mouse brains (Sekiguchi et al., 2009), and neuronal activity in the amygdala is regulated by GABAergic synapses. In *mdx* brain, the number of GABA-$_A$ receptors are reduced, resulting in reduced GABAergic synaptic transmission (Sekiguchi et al., 2009), thus it is possible that reduced inhibitory transmission is responsible for increased response to an associative cue. While dystrophin is also found in the hippocampus, a brain structure important for learning and memory, in particular spatial learning, hippocampal-dependent learning was assessed measuring long-term potentiation (LTP) noticed no difference in two hippocampal pathways: the Schaffer-commissural and performant pathway (Sesay et al., 1996) consistent with the lack of functional impairment reported here using the MWM task. This implies loss of Dp427 may not affect hippocampal-dependent tasks but my change neuronal circuits in the amygdala.

4.3 Generation of conditional brain-specific dystrophin knock-out mouse models

Given these findings, my final aim was to develop brain-specific dystrophin mouse models; one experimentally inducible, and one constitutively knocked out, to explore the involvement of dystrophin isoforms other than Dp427 on behavioural indices of cognition. I first assessed the tissue-specificity of three NestinCre promoters using two reporter lines with the aim of generating a mouse model capable of depleting all dystrophin species from the brain. As expected, all three

NestinCre constructs examined contained brain-specific enhancer elements (NestinCre, NestinCre^{ERT2} (5.1) and NestinCre^{ERT2} (SB). Two NestinCre constructs contain a muscle-specific enhancer element (NestinCre and NestinCreERT2 (5.1)). One construct (NestinCre^{ERT2} (SB)) showed recombination in the absence of TAM. This unexpected recombination could be the result of a robust promoter driving expression of CreER^{T2}, saturating the cytoplasm with CreERT2, resulting in its translocation into the nucleus where it causes recombination of the floxed gene.

Nestin is an intermediate filament protein expressed in neural stem cells of the developing central nervous system (CNS), as well as in myogenic precursor cells, tooth buds, limb buds, heart, testis and eye (Reynolds and Weiss, 1992; Sejersen and Lendahl, 1993; Kachinsky et al., 1995; Frojdman et al., 1997; Wroblewski et al., 1997; Yang et al., 2000). The nestin transgene contains a muscle-specific enhancer in the first intron and a brain-specific enhancer in the second intron, driving expression in the developing muscle and nervous system (figure 19; (Cheng et al., 2004). While NestinCre constructs are often referred to as muscle- or brain-specific, it is difficult to establish from the original papers whether they contain only the brain- or only the muscle-specific enhancer elements. Thus, I used reporter mice that contained R26R mT/mG or R26RYFP marker genes to determine specificity of Cre-mediated recombination.

The membrane-targeted double fluorescent marker system (mT/mG) allows for visualization of recombined and non-recombined cells (Muzumdar et al., 2007). In this marker system, tandem dimer tomato (mT) is flanked between two loxP sites and is expressed in the absence of Cre-mediated excision. Excision of mT places the downstream green fluorescent protein (mG) in frame (Muzumdar et al., 2007). In the R26R-YFP reporter, Cre recombinase excises a stop sequence to allow downstream EYFP expression in Cre-expressing tissues. I show

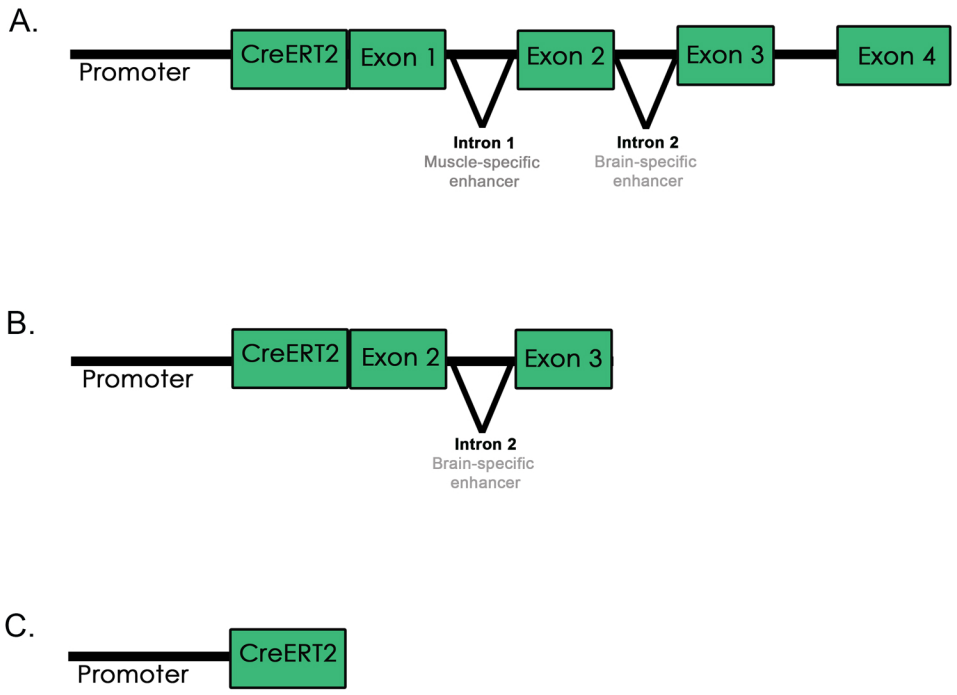

Figure 19 Location of brain and muscle enhancer elements in nestin promoter constructs. (A) Both muscle- and brain-specific enhancer elements are present. (B) Only brain-specific enhancer elements are present. (C) No enhancer elements are present. Figure adapted from Zimmerman *et al*, 1994.

here that of the three promoter constructs explored only the NestinCre^{ERT2} (SB) was exclusively brain-specific.

Unfortunately, none of these models depleted dystrophin from brain or muscle when crossed to a fDMDH mouse. As depicted in figure 20, the fDMDH mouse model has loxP sites that flank exons 2 -79 of murine DMD gene (unpublished). Since there is an inverse relationship between Cre-mediated efficiency and genetic distance (Zheng et al., 2000) it is likely that this deletion is simply too large for the Cre-recombinase enzyme to excise given that our reporter mice clearly demonstrate excellent recombination efficiency for loxP sites in close proximity.

4.4 Conclusion

In this thesis, hippocampal and amygdala cellular and behavioural phenotypes of *mdx* mice were characterized. The primary finding of this thesis is that ANSC symmetric division *in vitro* in *mdx* mice likely results in exhaustion of the population which is indicated by the reduction in primary and secondary NSP number. While this has no effect on *mdx* anxiety levels, repetitive behaviours as seen in ASD nor in spatial and reference memory, cue retention associative memory is enhanced (figure 21). Both hippocampus and amygdala are brain structures important for the acquisition and retention of memories (LeDoux, 2000; Crawley, 2007), but since the MWM is a hippocampal-dependent task it is likely that loss of Dp427 and the extent ANSC depletion in *mdx* mice does not impair hippocampal function. The behavioural improvement observed in FC suggests there are neurophysiological changes in the amygdala, a brain structure important for associative learning, and known to be affected by Dp427 loss (LeDoux, 2000; Crawley, 2007; Sekiguchi et al., 2009) possibly regulated by local GABAergic inhibition (Sekiguchi et al., 2009).

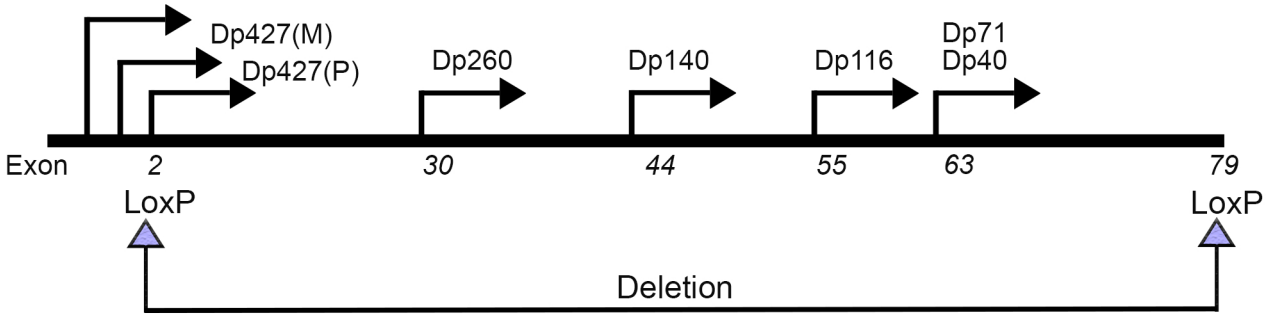

Figure 20 Location of the loxP sites designed to excise the DMD gene between exons 2 - 79 in the fDMDH mouse mode

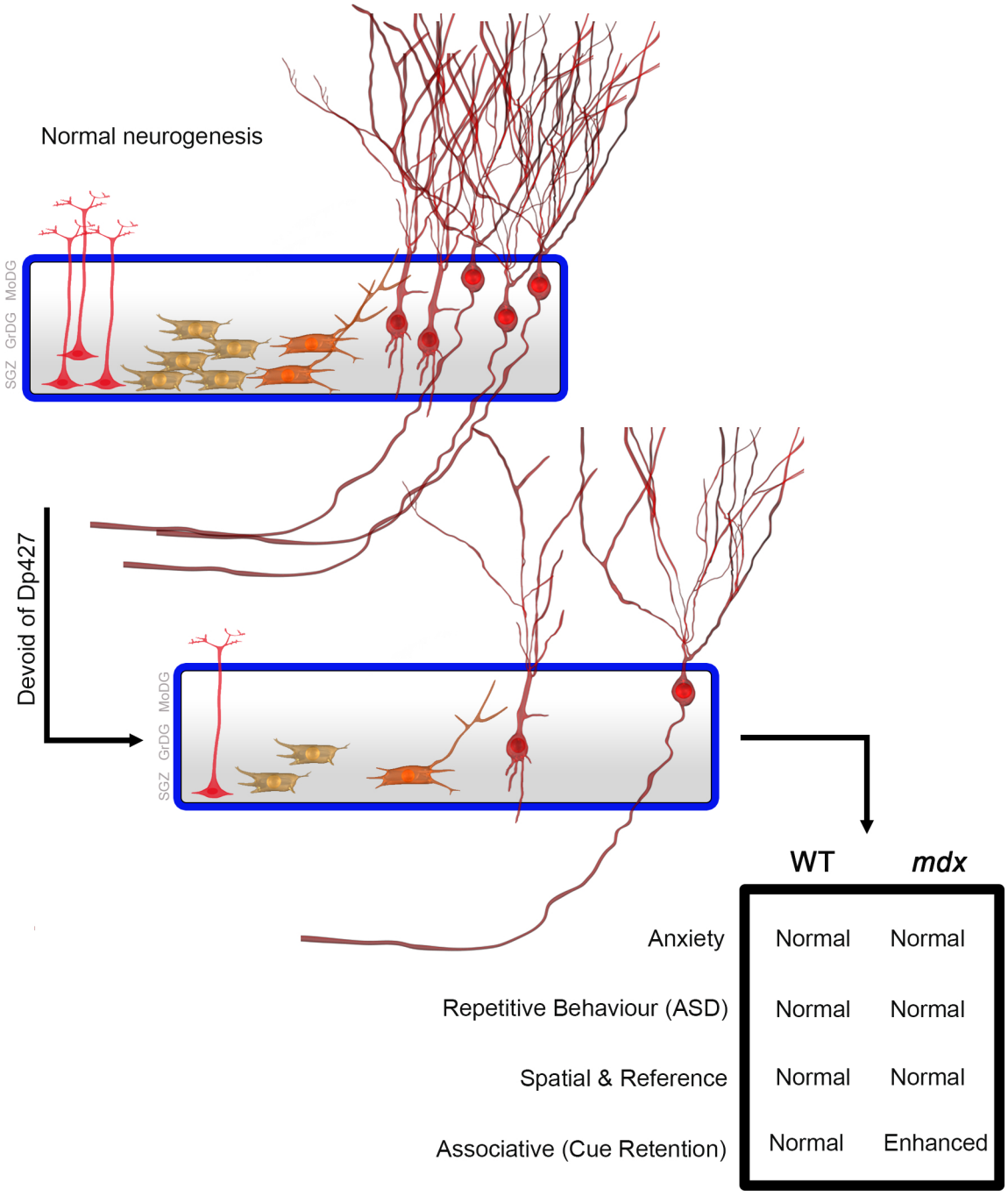

Figure 21 Proposed association between impaired neruogenesis due to ANSC depletion in the mdx mouse and changes on behavioural indices of cognition (or lack thereof) reported in this thesis. ANSC depletion, following initial increased proliferation, may result in fewer mature neurons being generated in *mdx* mice. This has no effect on *mdx* anxiety levels, repetitive behaviours modelling ASD, nor in spatial learnin and memory as assessed in the MWM. However, cue retention associative memory is enhanced in *mdx* mice.

Clearly, other isoforms must play a role in modulating cognitive impairment in DMD patients given the lack of any conclusive phenotype in a mouse model that depletes only Dp427. Thus, while the *mdx* mouse model is a valuable tool that has provided insight into both the muscle pathology and cognitive impairments affecting DMD patients (or lack thereof) future studies would benefit from focusing on generating mouse model that depletes all dystrophin isoforms in a brain-specific fashion.

5 REFERENCES

Anderson JL, Head SI, Rae C, Morley JW (2002) Brain function in Duchenne muscular dystrophy. Brain 125:4-13.

Angoa-Perez M, Kane MJ, Briggs DI, Francescutti DM, Kuhn DM (2013) Marble burying and nestlet shredding as tests of repetitive, compulsive-like behaviors in mice. J Vis Exp:50978.

Annese T, Corsi P, Ruggieri S, Tamma R, Marinaccio C, Picocci S, Errede M, Specchia G, De Luca A, Frassanito MA, Desantis V, Vacca A, Ribatti D, Nico B (2016) Isolation and characterization of neural stem cells from dystrophic mdx mouse. Exp Cell Res 343:190-207.

Banihani R, Smile S, Yoon G, Dupuis A, Mosleh M, Snider A, McAdam L (2015) Cognitive and Neurobehavioral Profile in Boys With Duchenne Muscular Dystrophy. J Child Neurol 30:1472-1482.

Belligni EF, Di Gregorio E, Biamino E, Calcia A, Molinatto C, Talarico F, Ferrero GB, Brusco A, Silengo MC (2012) 790 Kb microduplication in chromosome band 17p13.1 associated with intellectual disability, afebrile seizures, dysmorphic features, diabetes, and hypothyroidism. Eur J Med Genet 55:222-224.

Berube NG, Mangelsdorf M, Jagla M, Vanderluit J, Garrick D, Gibbons RJ, Higgs DR, Slack RS, Picketts DJ (2005) The chromatin-remodeling protein ATRX is critical for neuronal survival during corticogenesis. J Clin Invest 115:258-267.

Blake DJ (2002) Dystrobrevin dynamics in muscle-cell signalling: a possible target for therapeutic intervention in Duchenne muscular dystrophy? Neuromuscul Disord 12 Suppl 1:S110-117.

Blundell J, Blaiss CA, Etherton MR, Espinosa F, Tabuchi K, Walz C, Bolliger MF, Sudhof TC, Powell CM (2010) Neuroligin-1 deletion results in impaired spatial memory and increased repetitive behavior. J Neurosci 30:2115-2129.

Bond AM, Ming GL, Song H (2015) Adult Mammalian Neural Stem Cells and Neurogenesis: Five Decades Later. Cell Stem Cell 17:385-395.

Bresolin N, Castelli E, Comi GP, Felisari G, Bardoni A, Perani D, Grassi F, Turconi A, Mazzucchelli F, Gallotti D, et al. (1994) Cognitive impairment in Duchenne muscular dystrophy. Neuromuscul Disord 4:359-369.

Chang NC, Chevalier FP, Rudnicki MA (2016) Satellite Cells in Muscular Dystrophy - Lost in Polarity. Trends Mol Med 22:479-496.

Chaussenot R, Edeline JM, Le Bec B, El Massioui N, Laroche S, Vaillend C (2015) Cognitive dysfunction in the dystrophin-deficient mouse model of Duchenne muscular dystrophy: A reappraisal from sensory to executive processes. Neurobiol Learn Mem 124:111-122.

Cheng L, Jin Z, Liu L, Yan Y, Li T, Zhu X, Jing N (2004) Characterization and promoter analysis of the mouse nestin gene. FEBS Lett 565:195-202.

Cicero SA, Johnson D, Reyntjens S, Frase S, Connell S, Chow LM, Baker SJ, Sorrentino BP, Dyer MA (2009) Cells previously identified as retinal stem cells are pigmented ciliary epithelial cells. Proc Natl Acad Sci U S A 106:6685-6690.

Cohen HJ, Molnar GE, Taft LT (1968) The genetic relationship of progressive muscular dystrophy (Duchenne type) and mental retardation. Dev Med Child Neurol 10:754-765.

Cotton SM, Voudouris NJ, Greenwood KM (2005) Association between intellectual functioning and age in children and young adults with Duchenne muscular dystrophy: further results from a meta-analysis. Dev Med Child Neurol 47:257-265.
Crawley J (2007) What's wrong with my mouse? New Jersey, USA: Wiley.
Croona C, Kihlgren M, Lundberg S, Eeg-Olofsson O, Eeg-Olofsson KE (1999) Neuropsychological findings in children with benign childhood epilepsy with centrotemporal spikes. Dev Med Child Neurol 41:813-818.
D'Souza VN, Nguyen TM, Morris GE, Karges W, Pillers DA, Ray PN (1995) A novel dystrophin isoform is required for normal retinal electrophysiology. Hum Mol Genet 4:837-842.
Deacon RM (2006) Assessing nest building in mice. Nat Protoc 1:1117-1119.
Deacon RM, Thomas CL, Rawlins JN, Morley BJ (2007) A comparison of the behavior of C57BL/6 and C57BL/10 mice. Behav Brain Res 179:239-247.
Desguerre I, Mayer M, Leturcq F, Barbet JP, Gherardi RK, Christov C (2009) Endomysial fibrosis in Duchenne muscular dystrophy: a marker of poor outcome associated with macrophage alternative activation. J Neuropathol Exp Neurol 68:762-773.
DiMario JX, Uzman A, Strohman RC (1991) Fiber regeneration is not persistent in dystrophic (MDX) mouse skeletal muscle. Dev Biol 148:314-321.
Doorenweerd N, Mahfouz A, van Putten M, Kaliyaperumal R, PAC TH, Hendriksen JGM, Aartsma-Rus AM, Verschuuren J, Niks EH, Reinders MJT, Kan HE, Lelieveldt BPF (2017) Timing and localization of human dystrophin isoform expression provide insights into the cognitive phenotype of Duchenne muscular dystrophy. Sci Rep 7:12575.
Duchenne GB (1868) Recherces sur lab paralysie musculaire pseudo-hypertrophique, ou paralysie myo-sclerosique. Arch Gen Med 6:569.
Dumont NA, Wang YX, von Maltzahn J, Pasut A, Bentzinger CF, Brun CE, Rudnicki MA (2015) Dystrophin expression in muscle stem cells regulates their polarity and asymmetric division. Nat Med 21:1455-1463.
Ehmsen J, Poon E, Davies K (2002) The dystrophin-associated protein complex. J Cell Sci 115:2801-2803.
Fowler SL, Akins M, Zhou H, Figeys D, Bennett SA (2013) The liver connexin32 interactome is a novel plasma membrane-mitochondrial signaling nexus. J Proteome Res 12:2597-2610.
Frojdman K, Pelliniemi LJ, Lendahl U, Virtanen I, Eriksson JE (1997) The intermediate filament protein nestin occurs transiently in differentiating testis of rat and mouse. Differentiation 61:243-249.
Granger MW, Franko B, Taylor MW, Messier C, George-Hyslop PS, Bennett SA (2016) A TgCRND8 Mouse Model of Alzheimer's Disease Exhibits Sexual Dimorphisms in Behavioral Indices of Cognitive Reserve. J Alzheimers Dis 51:757-773.
Hendriksen JG, Vles JS (2008) Neuropsychiatric disorders in males with duchenne muscular dystrophy: frequency rate of attention-deficit hyperactivity disorder (ADHD), autism spectrum disorder, and obsessive--compulsive disorder. J Child Neurol 23:477-481.
Hinton VJ, De Vivo DC, Nereo NE, Goldstein E, Stern Y (2000) Poor verbal working memory across intellectual level in boys with Duchenne dystrophy. Neurology 54:2127-2132.
Hollinger K, Selsby JT (2013) The physiological response of protease inhibition in dystrophic muscle. Acta Physiol (Oxf) 208:234-244.

Im WB, Phelps SF, Copen EH, Adams EG, Slightom JL, Chamberlain JS (1996) Differential expression of dystrophin isoforms in strains of mdx mice with different mutations. Hum Mol Genet 5:1149-1153.
Imayoshi I, Ohtsuka T, Metzger D, Chambon P, Kageyama R (2006) Temporal regulation of Cre recombinase activity in neural stem cells. Genesis 44:233-238.
Imbeault S, Gauvin LG, Toeg HD, Pettit A, Sorbara CD, Migahed L, DesRoches R, Menzies AS, Nishii K, Paul DL, Simon AM, Bennett SA (2009) The extracellular matrix controls gap junction protein expression and function in postnatal hippocampal neural progenitor cells. BMC Neurosci 10:13.
Ito K, Suda T (2014) Metabolic requirements for the maintenance of self-renewing stem cells. Nat Rev Mol Cell Biol 15:243-256.
Jensen JB, Parmar M (2006) Strengths and limitations of the neurosphere culture system. Mol Neurobiol 34:153-161.
Kachinsky AM, Dominov JA, Miller JB (1995) Intermediate filaments in cardiac myogenesis: nestin in the developing mouse heart. J Histochem Cytochem 43:843-847.
Kempermann G, Jessberger S, Steiner B, Kronenberg G (2004) Milestones of neuronal development in the adult hippocampus. Trends Neurosci 27:447-452.
Klingler W, Jurkat-Rott K, Lehmann-Horn F, Schleip R (2012) The role of fibrosis in Duchenne muscular dystrophy. Acta Myol 31:184-195.
Krasowska E, Zablocki K, Gorecki DC, Swinny JD (2014) Aberrant location of inhibitory synaptic marker proteins in the hippocampus of dystrophin-deficient mice: implications for cognitive impairment in duchenne muscular dystrophy. PLoS One 9:e108364.
Kronenberg G, Reuter K, Steiner B, Brandt MD, Jessberger S, Yamaguchi M, Kempermann G (2003) Subpopulations of proliferating cells of the adult hippocampus respond differently to physiologic neurogenic stimuli. J Comp Neurol 467:455-463.
LeDoux JE (2000) Emotion circuits in the brain. Annu Rev Neurosci 23:155-184.
Lenk U, Hanke R, Thiele H, Speer A (1993) Point mutations at the carboxy terminus of the human dystrophin gene: implications for an association with mental retardation in DMD patients. Hum Mol Genet 2:1877-1881.
Lidov HG (2000) The molecular neuropathology of the muscular dystrophies: a review and update. J Neuropathol Exp Neurol 59:1019-1030.
Lise MF, El-Husseini A (2006) The neuroligin and neurexin families: from structure to function at the synapse. Cell Mol Life Sci 63:1833-1849.
Manning J, Kulbida R, Rai P, Jensen L, Bouma J, Singh SP, O'Malley D, Yilmazer-Hanke D (2014) Amitriptyline is efficacious in ameliorating muscle inflammation and depressive symptoms in the mdx mouse model of Duchenne muscular dystrophy. Exp Physiol 99:1370-1386.
Mateus-Pinheiro A, Pinto L, Sousa N (2011) Epigenetic (de)regulation of adult hippocampal neurogenesis: implications for depression. Clin Epigenetics 3:5.
McGreevy JW, Hakim CH, McIntosh MA, Duan D (2015) Animal models of Duchenne muscular dystrophy: from basic mechanisms to gene therapy. Dis Model Mech 8:195-213.
Mehler MF (2000) Brain dystrophin, neurogenetics and mental retardation. Brain Res Brain Res Rev 32:277-307.
Miranda R, Laroche S, Vaillend C (2016) Reduced neuronal density in the CA1 anterodorsal hippocampus of the mdx mouse. Neuromuscul Disord 26:775-781.

Miranda R, Nagapin F, Bozon B, Laroche S, Aubin T, Vaillend C (2015) Altered social behavior and ultrasonic communication in the dystrophin-deficient mdx mouse model of Duchenne muscular dystrophy. Mol Autism 6:60.
Morgan JE, Partridge TA (2003) Muscle satellite cells. Int J Biochem Cell Biol 35:1151-1156.
Muntoni F, Mateddu A, Serra G (1991) Passive avoidance behaviour deficit in the mdx mouse. Neuromuscul Disord 1:121-123.
Muntoni F, Cau M, Congiu R, Congia M, Cao A, Melis MA (1993) Identification of a novel T-insertion polymorphism at the DMD locus. Hum Genet 92:103.
Muzumdar MD, Tasic B, Miyamichi K, Li L, Luo L (2007) A global double-fluorescent Cre reporter mouse. Genesis 45:593-605.
Neumuller RA, Knoblich JA (2009) Dividing cellular asymmetry: asymmetric cell division and its implications for stem cells and cancer. Genes Dev 23:2675-2699.
Nishio H, Takeshima Y, Narita N, Yanagawa H, Suzuki Y, Ishikawa Y, Ishikawa Y, Minami R, Nakamura H, Matsuo M (1994) Identification of a novel first exon in the human dystrophin gene and of a new promoter located more than 500 kb upstream of the nearest known promoter. J Clin Invest 94:1037-1042.
Nudel U, Zuk D, Einat P, Zeelon E, Levy Z, Neuman S, Yaffe D (1989) Duchenne muscular dystrophy gene product is not identical in muscle and brain. Nature 337:76-78.
Pangalila RF, van den Bos GA, Bartels B, Bergen M, Stam HJ, Roebroeck ME (2015) Prevalence of fatigue, pain, and affective disorders in adults with duchenne muscular dystrophy and their associations with quality of life. Arch Phys Med Rehabil 96:1242-1247.
Rahman M, Reyner K, Deleyrolle L, Millette S, Azari H, Day BW, Stringer BW, Boyd AW, Johns TG, Blot V, Duggal R, Reynolds BA (2015) Neurosphere and adherent culture conditions are equivalent for malignant glioma stem cell lines. Anat Cell Biol 48:25-35.
Remmelink E, Aartsma-Rus A, Smit AB, Verhage M, Loos M, van Putten M (2016) Cognitive flexibility deficits in a mouse model for the absence of full-length dystrophin. Genes Brain Behav 15:558-567.
Reynolds BA, Weiss S (1992) Generation of neurons and astrocytes from isolated cells of the adult mammalian central nervous system. Science 255:1707-1710.
Sejersen T, Lendahl U (1993) Transient expression of the intermediate filament nestin during skeletal muscle development. J Cell Sci 106 (Pt 4):1291-1300.
Sekiguchi M, Zushida K, Yoshida M, Maekawa M, Kamichi S, Yoshida M, Sahara Y, Yuasa S, Takeda S, Wada K (2009) A deficit of brain dystrophin impairs specific amygdala GABAergic transmission and enhances defensive behaviour in mice. Brain 132:124-135.
Sesay AK, Errington ML, Levita L, Bliss TV (1996) Spatial learning and hippocampal long-term potentiation are not impaired in mdx mice. Neurosci Lett 211:207-210.
Silverman JL, Yang M, Lord C, Crawley JN (2010) Behavioural phenotyping assays for mouse models of autism. Nat Rev Neurosci 11:490-502.
Snow WM, Anderson JE, Jakobson LS (2013) Neuropsychological and neurobehavioral functioning in Duchenne muscular dystrophy: a review. Neurosci Biobehav Rev 37:743-752.
Sun SC, Peng YS, He JB (2008) [Changes of serum creatine kinase levels in children with Duchenne muscular dystrophy]. Zhongguo Dang Dai Er Ke Za Zhi 10:35-37.
Swayne LA, Bennett SA (2016) Connexins and pannexins in neuronal development and adult neurogenesis. BMC Cell Biol 17 Suppl 1:10.

Takos AM, Rook F (2013) Towards a molecular understanding of the biosynthesis of amaryllidaceae alkaloids in support of their expanding medical use. Int J Mol Sci 14:11713-11741.
Uchino M, Teramoto H, Naoe H, Yoshioka K, Miike T, Ando M (1994) Localisation and characterisation of dystrophin in the central nervous system of controls and patients with Duchenne muscular dystrophy. J Neurol Neurosurg Psychiatry 57:426-429.
Vaillend C, Billard JM, Laroche S (2004) Impaired long-term spatial and recognition memory and enhanced CA1 hippocampal LTP in the dystrophin-deficient Dmd(mdx) mouse. Neurobiol Dis 17:10-20.
Vaillend C, Rendon A, Misslin R, Ungerer A (1995) Influence of dystrophin-gene mutation on mdx mouse behavior. I. Retention deficits at long delays in spontaneous alternation and bar-pressing tasks. Behav Genet 25:569-579.
Vaillend C, Billard JM, Claudepierre T, Rendon A, Dutar P, Ungerer A (1998) Spatial discrimination learning and CA1 hippocampal synaptic plasticity in mdx and mdx3cv mice lacking dystrophin gene products. Neuroscience 86:53-66.
van Putten M, Hulsker M, Nadarajah VD, van Heiningen SH, van Huizen E, van Iterson M, Admiraal P, Messemaker T, den Dunnen JT, t Hoen PA, Aartsma-Rus A (2012) The effects of low levels of dystrophin on mouse muscle function and pathology. PLoS One 7:e31937.
Waite A, Tinsley CL, Locke M, Blake DJ (2009) The neurobiology of the dystrophin-associated glycoprotein complex. Ann Med 41:344-359.
Walker TL, Kempermann G (2014) One mouse, two cultures: isolation and culture of adult neural stem cells from the two neurogenic zones of individual mice. J Vis Exp:e51225.
Wicksell RK, Kihlgren M, Melin L, Eeg-Olofsson O (2004) Specific cognitive deficits are common in children with Duchenne muscular dystrophy. Dev Med Child Neurol 46:154-159.
Wroblewski J, Engstrom M, Edwall-Arvidsson C, Sjoberg G, Sejersen T, Lendahl U (1997) Distribution of nestin in the developing mouse limb bud in vivo and in micro-mass cultures of cells isolated from limb buds. Differentiation 61:151-159.
Yang J, Bian W, Gao X, Chen L, Jing N (2000) Nestin expression during mouse eye and lens development. Mech Dev 94:287-291.
Zhao C, Deng W, Gage FH (2008) Mechanisms and functional implications of adult neurogenesis. Cell 132:645-660.
Zheng B, Sage M, Sheppeard EA, Jurecic V, Bradley A (2000) Engineering mouse chromosomes with Cre-loxP: range, efficiency, and somatic applications. Mol Cell Biol 20:648-655.